DEVELOPMENT OF SENSING TECHNOLOGIES BASED ON OPTICAL FIBRE FROM A NEW APPROACH

by

Oskar Arrizabalaga

A dissertation submitted
to the School of Engineering of Bilbao
in partial fulfillment of the requeriments
for the degree of

PhD of Engineering

at the
UNIVERSITY OF THE BASQUE COUNTRY

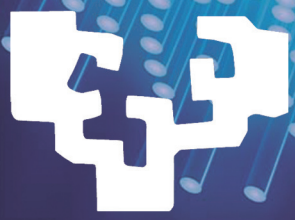

November, 2020

Contents

1 Overview

1.1 Introduction

Sensors connect the physical world to the world of electrical devices. Historically, advancements in materials science and engineering have been important drivers in the development of sensor technologies. For instance, the temperature sensitivity of electrical resistance in a variety of materials was noted in the early 1800s and was applied by Wilhelm von Siemens in 1860 to develop a temperature sensor based on a copper resistor. Today, sensors have become pervasive and essential in the modern industrial world. Applications range from sophisticated industrial processes to common consumer products. In many respects, the manufacturing industry has led the use of advanced sensors in monitoring and controlling its industrial processes.

As per industry reports, sensors are becoming the biggest and fastest growing markets, comparable with computers and communication devices markets. For instance, according to a BBC Research report, the global sensor market is chasing double-digit growth. It expects the global market for sensors to reach $240.3 billion in 2021, up from about $12.5 billion in 2016. Fingerprint sensors will lead the market by growing at 15.9 per cent annually. Another source puts chemical sensors, process variable sensors, proximity and positioning sensors among the fastest growing markets. Automotive industry will once again be the leading consumer market for sensors. It is also important to highlight that biomedical sensors market was valued at $10.79 billion in 2019 and is expected to reach $15.13 billion by 2025, at a Compound Annual Growth Rate (CAGR) of 6% over the forecast period 2020 – 2025. As well as, aircraft sensors market is also projected to grow from $3.8 billion in 2019 to $4.9 billion by 2025, at a CAGR of 4.48 % from 2019 to 2025.

By definition, a sensor is a device that senses the physical changes occuring in its surrounding and converts them it into a readable quantity. Therefore, its function consists in detecting the changes and inducing the corresponding electrical signal. This electrical value can be in the form of voltage, current, or charge and can be channelled, amplified, and modified by electronic devices. In others words, a sensor has input properties and electrical output properties.

The term sensor should be distinguished from transducer. The latter is an electrical device that is used to convert one form of energy into another form, whereas the former, converts changes in the physical attributes of the non-electrical signal into an electrical signal that can be easily measurable. The process of energy conversion in the transducer is known as the transduction. The

transduction consist in two steps. First, sensing the signal, and then, strengthening it for further processing. Transducers may be parts of more complex sensors. For instance, a chemical sensor may have a part which converts the energy of a chemical reaction into heat, and another part, a thermopile, which converts heat into an electrical signal. The combination of both parts forms a chemical sensor, a device which produces an electrical signal in response to a chemical reaction.

In general, sensor types are classified as direct and complex. A direct sensor converts a nonelectrical stimulus into an electrical signal or modifies an electrical signal by using an appropriate physical effect, whereas a complex sensor requires of several transformation steps before the electric output signal can be generated. These steps consist in several changes of the types of energy, where the final step must produce an electrical signal of a desirable format. For example, the displacement of an opaque object can be detect/measure, by means of a fibre optic sensor. A excitation signal generated by a light source is transmitted via an optical fibre to the target and reflected from its surface. This reflected light, is collected by the optical fibre itself and guided to a photodiode, where it produces an electric current, which represent the distance from the end of the fibre optic to the target. Therefore, such a sensing process includes two energy conversion steps and a manipulation of the optical signal as well.

Thermoelectric (Seebeck) effect, magnetism, piezoelectricity, or the photoeffect are some examples of physical effects that result in the direct generation of electrical signal in response to nonelectrical influences. Consequently, many sensing technologies based on the aforementioned and others effects have been developed. The following list contains the physical sensing principles based on the physical effects that can be used for a direct conversion of stimuli into electric signals.

- Electric charges, fields and potentials
- Capacitive sensing
- Magnetic sensing
- Electromagnetic sensing
- Inductive sensing
- Resistive sensing
- Piezoelectric sensing
- Photoelectric sensing
- Hall effect
- Thermoelectric sensing
- Sound waves
- Thermal properties of materials
- Heat transfer
- Light sensing

Today in practically every branch of industry, sensors devices have become indispensable. In fact, there is hardly any industrial area that can do without measuring, testing, monitoring, or automation.

Aerospace, automotive, entertainment, medical and security are examples of industries where sensors have become essential. The value chain extends from detection of process parameters in process technology to the analysis of product characteristics in the entire productive industry. With the help of sensor technology, the ability to manufacture products with unique features, but without significantly increasing production costs, is becoming increasingly successful.

Technologies such as microelectromechanical systems (MEMS) [1–3], complementary metal-oxide-semiconductor (CMOS) [4, 5] or nanoelectromechanical systems (NEMS) [6] are fundamental pillars for developing sensors with increasing capabilities and greater functionalities. Among their many advantages are high sensitivity, possibility of integration with microelectronics to achieve embedded mechatronic systems or very low power consumption. Additionally, scaling effects at microscopic levels can be exploited to achieve designs and dynamic mechanisms otherwise not possible at macro-scales. However, the expensive cost during the research and development stage for any new design or device, the very expensive upfront setup cost for fabrication cleanrooms and foundry facilities and the fact of testing equipment to characterise the quality and performance, are the main disadvantages of these technologies. As well as, the fabrication and assembly unit costs can be very high for low quantities.

In addition, the use of more complex and automated systems, having to comply with many norms related to low energy consumption, miniaturization, insensitivity to modifications of the surrounding conditions, security, etc. has induced the need of a new generation of sensors that have to be reliable, low cost, easy to produce, if possible without clean rooms and avoiding too demanding calibration.

Overcoming the above needs gave rise to an alternative to the microelectronic-based sensors, those based on optical fibres (OFs) [7]. These type of sensors, due to the several advantages, which include lightweight, immunity to electromagnetic interference, large bandwidth, high sensitivity or ease in implementing distributed sensors, are undoubtedly intended to play a key role in driving the advancement of these requirements.

Nowadays, fibre optic sensing technology provides a range of solutions for growing range of applications in areas ranging from structural health monitoring to biophotonic sensing, to name a few. However, with a few exceptions, they have not yet achieved the set of needs that the market demands to be stablished

commercially. The development of new materials and advances in physics and chemistry together with a new variety of optical fibres, will allow us to discover new phenomena to stimulate the development of a new generation of sensors.

Optical techniques have expanded significantly in the last few years and, therewith optical fibre-based sensors. The key to the advancement of this type of sensors has been the optoelectronic devices developed for the telecommunications industry. They have been able to capitalize on the use of a wide availability of high-quality optical and electronic components associated with optical fibres at competitive prices. In addition to a large number of new fibres is nowadays available with different materials and geometries [8].

The field of optical fibres has undergone growing up and advancement over the last three decades. Although these were initially conceived as a mean of transmitting light and images for endoscopic medical applications, later, in the mid-1960s, they were proposed as a suitable means of transporting information for telecommunications applications [9]. Ever since, optical fibres has been the subject of intensive effort on research and development to the point that today light wave communication systems have become the preferred method of transmitting large amounts of data and information from one point to another. The great success of optical fibres in telecommunications together with their several advantages such as high bandwidth, immunity to electromagnetic interference, small size, light weight, safety, and relatively low cost, has generated numerous applications in a number of related fields, such as sensing, biophotonics and high-power lasers. The topic remains extraordinarily buoyant and new materials, structure and applications emerge unabated.

Optical fibre sensors (OFSs) rely on communication technology to provide a basic set of components and also to facilitate specialised technologies through which slightly different versions of fibre optics can be fabricated exclusively for the sensing community. Semiconductor sources, and detectors, fibre components such as couplers, splitters, wavelength multiplexors, and a lot of other photonic devices, as well as handling and test procedures, could not have been realised without the communication stimulus.

There are numerous embodiments of OFSs, but they all fall into two broad categories. For some sensors, the fibre acts as a light guide to a sensing region where the optical signal emerges into another medium within which it is modulated. The light is then collected by the same or a different fibre after it has been modulated by the measurand and returned to a remote location for processing. This type of OFSs are denominated as extrinsic sensors. In contrast, intrinsic sensors keep the light within the fibre at all times so that the external parameter of interest modulates the light as it propagates along the fibre. Both types have

made some inroads into the commercial application with extrinsic sensors being predominantly targeted at chemical and biomedical measurements and intrinsic sensors focused especially on physical measurements.

The early work in fibre sensing focused on measuring the physical parameters at a particular point. However, the research community gradually realised that if it is possible to influence the transmission properties of an optical fibre through external parameters, then it is also possible to measure this parameter field based on the position along the fibre. This feature, called distributed measurements have become an important differentiator of fibre sensor technology. In fact, the technical capacity to perform distributed measurements over distances of up to several tens of kilometres are exclusive to optical fibres. Electronic-based gauge lengths are commonly on the order of one meter, and there are some that go to even shorter discrimination lengths.

However, despite the different types of OFSs that exist on the market, they are not as well known today as their electronic counterparts. There are some barriers such as price, size, sensitivity or operating range that these sensors have to overcome to be competitive in the industrial market. Actually, the interferometry based on optical fibres appears as the most efficient way to enhance sensor sensitivity and its detection limit. This leads to the area of micro -and nano-engineered optical sensors. The combination of better fabrication techniques and new physical effects will open up new market niches in may areas of the industry of the future.

Traditional bulk optic components such as beam splitters, combiners, and objective lenses have been rapidly replaced by small-sized fiber devices that enable the sensors to operate on fibre scales. Thus, interferometry is the best technology to develop miniaturized optical fibre sensors. As well as, this sensing technology offers several advantages such as easy alignment, high coupling efficiency, and high stability.

On this basis, the work of this thesis demonstrates a new sensing technology to fabricate interferometric sensor devices that address relevant drawbacks such as miniaturization, high sensitivity and wide operating range, among others. Furthermore, they are suitable for multiple sensing applications.

The transducer of the devices presented in this thesis consists of an off-center polymer micro-cap bonded onto single mode fiber (SMF) tip. The SMF end face can be cleaved with a small angle or polished flat. The off-center causes an axial misalignment between the core of the fibre and the polymer micro-cap. Then, by adjusting this missaligment, it is possible to control the coupling coefficient and thus, the reflection of the interface between the polymer and the external medium, allowing to optimize the fringe contrast of the interference pattern.

To evaluate experimentally the tecnology reported in this thesis, several samples were fabricated and they were experimentally evaluated as temperature, index meter and humidity sensor.

In the first manuscript reported in this thesis titled "*Accurate microthermometer based on off center polymer caps onto optical fiber tips*", it is presented a new approach to fabricate miniature and high-quality sensor devices based on an optical fibre. Once fabricated, they were evaluated as temperature sensors. The micro-caps were first encapsulated in a short piece of capillary tube in order to isolate the micro-cap from others physical parameters. After that, they were placed inside a mini temperature chamber equipped with a temperature controller. As a reference, a calibrated commercial RTD -resistance temperature detector- was placed in the mini temperature chamber close to the micro-cap. The experimental testing process was automatised, by implementing an ad-hoc LabVIEW program to control the temperature inside the chamber.

Thanks to the high thermal expansion coefficient of the polymer with which the micro-caps were made, these devices as a temperature sensor shown a sensitivity up to 270 pm/°C with a thermal response time of around 2.5 s. Furthermore, the high quality of the interference pattern has allowed to achieve a resolution of 0.04 °C. In addition, their simple fabrication process and their broad operating wavelength range (from 800 to 1600 nm, approximately) of these devices, along with the diversity of polymers currently available, make the concept and approach proposed here appealing, not only for measuring temperature, but also for sensing many others parameters.

In the next manuscript presented in this thesis, entitled "Microrefractometer Based on Off-Center Polymer Caps Bonded Onto Optical Fiber Tips", it is demonstrated that the interferometric micro-cap can also be used to sense changes in the index of the micro-cap's outer environment. The measuring index range of these sensor devices is from 1 up to the index of the polymer from which the microcap is made off. The sensitivity of these index meters was found to be $\approx 10^{-4}$ over the whole measuring range.

Finally, the research manuscript entitled "*Miniature interferometric humidity sensor based on an off-center polymer cap onto optical fiber facet*" consolidates the multiple applicability of the sensor device proposed in this thesis. The capability of polymers to absorb water molecules makes the polymer micro-cap a high sensitive transducer for humidity sensing applications. Fabricated samples were tested in a calibrated climatic chamber.

In addition to all this, the theoretical knowledge of the coupling coefficient in multicore fibres developed in this thesis has allowed to adequately control it, not only for the applications proposed in this thesis, but also for many others.

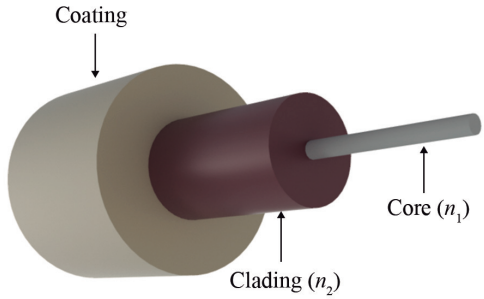

Figure 1: Structure of a standard optical fibre.

For example, with suitable polymers that can be bonded on the cleaved end of an optical fibre, this technology could be used in sensing applications that require detecting parameters, such as gases, pressure, humidity, etc.

Other possible applications can be found in the field of bio-chemical sensing. In these applications, synthetized polymers with tailored optical and physical properties will be required. Then, under the presence of the parameters to sense, the interference pattern will change, and therefore will be detected or monitored with the techniques proposed in this thesis. In addition, its fabrication process could be carried out automatically in a short time. In addition, the sensor benefits from high repeatability with low-cost, and straightforward and reproducible fabrication.

1.2 Theoretical Framework

Briefly, a standard fibre is composed of three main components: the core, the cladding, and the coating, as shown in Fig.1 The cladding has a lower refractive index (n_2) than the core (n_1). This index difference causes total internal reflection at the limit of the index along the length of the fibre so that the light remains confined within the core [10]. Therefore, the core is the light-transmitting component of an optical fibre. The coating serves to protect the fibre from external conditions and physical damage. Fundamentally, an optical fibre sensor works by modulating one or more properties of a propagating light wave, including intensity, phase, polarization, and frequency, in response to the environmental parameter being measured.

In its simplest form, an optical fibre sensor is composed of a light source, optical fibre, sensing element, and detector. There are many approaches to fibre-

based sensing which have made the greatest contributions to the development of OFSs. The main optical fibre-based techniques used to develop sensor devices are described below.

Light Modulation Techniques

The light that propagates along an optical fibre can be characterised by its intensity, phase, wavelength and polarization. When the fibre environment experiences a change, at least one of these parameters changes accordingly. By analysing this change, useful information can be obtained. Then, the efficiency of a fibre optic sensor depends on its ability to reliably and accurately convert changes in those parameters. Therefore, depending on the light modulation and effect used to measure physical phenomena, different sensing modulation techniques have been developed.

Intensity-based Light Modulation. Intensity-based OFSs rely on signal undergoing some loss. They are based on relating the amount of force or deformation applied to the fibre with the signal attenuation [11]. Other ways to attenuate the signal is through absorption or scattering of a target [12]. This technology requires more light and therefore usually uses multimode optical fibres [13].

There are a variety of mechanisms such as micro-bending loss, attenuation, and evanescent fields that can produce a measurand-induced change in the optical intensity propagated by an optical fibre. For example, an intensity-based micro-bending sensor consists of periodic mechanical micro-curves that cause the energy of the guided modes to be coupled to the radiation modes, and consequently the transmitted light is attenuated [14].

Another type of intensity based fibre optic sensor is the evanescent wave sensor that uses the light energy which leaks from the core into the cladding. These sensors are widely used as chemical sensors [15]. The sensing is accomplished by stripping the cladding from a section of the fibre and using a light source having a wavelength that can be absorbed by the chemical that is to be detected [16]. The resulting change in light intensity is a measure of the chemical concentration. Measurements can also be performed in a similar method by replacing the cladding with a material such as an organic dye whose optical properties can be changed by the chemical under investigation.

The advantages of these OFSs are the simplicity of implementation, low cost, possibility of being multiplexed, and ability to perform as real distributed sensors. However, relative measurements and that variations in the intensity of

the light source may lead to false readings unless a referencing system is used, are their main drawbacks.

Interferometric-based Light Modulation. Optical interference corresponds to the interaction of two or more light waves that produce a resulting irradiance that deviates from the sum of the component irradiances. According to the superposition principle, the resultant electric-field intensity space where two or more lightwaves overlap, is equal to the vector sum of the individual constituent disturbances. Then, the electric field intensity $\overrightarrow{\mathbf{E}}$ at a point in space, arising from the separate fields of various contributing sources is given by [17]

$$\overrightarrow{\mathbf{E}} = \overrightarrow{\mathbf{E}}_1 + \overrightarrow{\mathbf{E}}_2 + ... \tag{1}$$

However, the optical disturbance, or light field $\overrightarrow{\mathbf{E}}$, varies in time at an extremely fast rate, making the actual field an impractical quantity to detect. Instead, the irradiance can be measured directly with a wide variety of sensors. The study of interference, is therefore best approached by way of the irradiance.

Let us consider only linearly polarized waves of the form

$$\overrightarrow{\mathbf{E}}_1(\overrightarrow{r}, t) = \overrightarrow{\mathbf{E}}_{01} \cos\left(\overrightarrow{\mathbf{K}}_1 \overrightarrow{r} - \omega t + \phi_1\right) \tag{2}$$

and

$$\overrightarrow{\mathbf{E}}_2(\overrightarrow{r}, t) = \overrightarrow{\mathbf{E}}_{02} \cos\left(\overrightarrow{\mathbf{K}}_2 \overrightarrow{r} - \omega t + \phi_2\right). \tag{3}$$

The irradiance is given by

$$I = \langle \overrightarrow{\mathbf{E}}^2 \rangle_T, \tag{4}$$

where

$$\overrightarrow{\mathbf{E}}^2 = \overrightarrow{\mathbf{E}} \cdot \overrightarrow{\mathbf{E}}$$

and

$$\overrightarrow{\mathbf{E}}^2 = (\overrightarrow{\mathbf{E}}_1 + \overrightarrow{\mathbf{E}}_2) \cdot (\overrightarrow{\mathbf{E}}_1 + \overrightarrow{\mathbf{E}}_2) = \overrightarrow{\mathbf{E}}_1^2 + \overrightarrow{\mathbf{E}}_2^2 + 2\overrightarrow{\mathbf{E}}_1 \cdot \overrightarrow{\mathbf{E}}_2.$$

Therefore, the irradiance becomes

$$\overrightarrow{\mathbf{E}}^2 = \overrightarrow{\mathbf{E}}_1^2 + \overrightarrow{\mathbf{E}}_2^2 + 2\overrightarrow{\mathbf{E}}_1 \cdot \overrightarrow{\mathbf{E}}_2$$

taking the time average of both sides, we find that

$$I = I_1 + I_2 + I_{12} \tag{5}$$

where

$$I_1 = \langle \overrightarrow{\mathbf{E}}_1^2 \rangle_T = \frac{\overrightarrow{\mathbf{E}}_{01}^2}{2} \tag{6}$$

$$I_2 = \langle \overrightarrow{\mathbf{E}}_1^2 \rangle_T = \frac{\overrightarrow{\mathbf{E}}_{02}^2}{2} \tag{7}$$

$$I_{12} = 2\langle \overrightarrow{\mathbf{E}}_1 \cdot \overrightarrow{\mathbf{E}}_2 \rangle_T = 2\sqrt{I_1 I_2}\cos\delta, \tag{8}$$

thus, the irradiance

$$I_T = I_1 + I_2 + 2\sqrt{I_1 I_2}\cos\delta \tag{9}$$

where δ is the phase difference arising from a combined path length and initial phase-angle difference. Irradiance maxima are obtained when $\delta = \pm 2m\pi$, and irradiance minima when $\delta = \pm(2m+1)\pi$.

Interferometry-based optical sensors use changes in δ as the sensing principle. They can be categorized into four types: Mach-Zehnder, Michelson, Sagnac and Fabry-Perot. By modulating these techniques it is possible to sense several physical parameters such as temperature, strain, pressure, refractive index and so on [18–21].

Mach Zehnder Interferometer. OFSs based on a Mach-Zehnder interferometer [22, 23] (MZI) consist of two independent arms, which are typically named the sensing arm, with physical length L_S, and the reference arm, with physical length L_R. In many transducers the reference arm is kept isolated from environment and only the sensitive window is exposed to the measurand. This is not a requirement, since in some transducers both arms are used for sensing in either differential or push–pull configurations to double the sensitivity of the transducer or for gradiometer applications. The difference in the two path lengths, $L_R - L_S$, is the mismatch of the physical path. These type of sensors are compact and robust and, depending on the losses of the optical fibre, the sensor can be a few meters or several kilometers, with little impact on the performance of the sensor.

When a light beam is divided into two arms with irradiances I_1 and I_2 using a fibre coupler and then recombined by means of another fibre coupler as it can be seen in Fig.2, the irradiance of the recombined light I_T, can be calculated from Eq.9.

In general, the reference arm is kept isolated from external variation and only the sensitive window is exposed to the parameter to be detected. Therefore, changes in length L, in the effective index n_{eff}, or both (due to the measurand), result into a phase shift δ which is calculated as

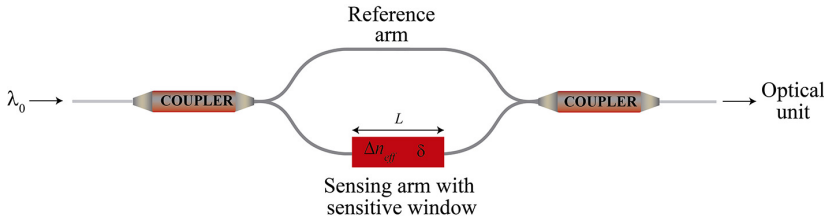

Figure 2: Schematic representation of the Mach Zehnder interferometer.

$$\delta = \frac{2\pi}{\lambda_0} \Delta n_{\text{eff}} L, \tag{10}$$

being λ the wavelength of light in vacuum and Δn_{eff} the index variation caused by the measurand. From Eq.10 it can be deduced that the maximum values of the recombined intensity are found at wavelengths $\lambda_m = \Delta n_{\text{eff}} L/m$ ($m \in \mathbb{N} \neq 0$). From the latter, it can be seen that either Δn_{eff} or L get affected by the environment so that the sensor will lead to a shift in the interference pattern. The distance between two consecutive maxima can be calculated as

$$\Delta\lambda_m = \frac{\Delta n_{\text{eff}} L}{m-1} \tag{11}$$

so, the calculation of the Free Spectral Range, FSR, can be approximated to

$$FSR_{MZI} \approx \frac{\lambda^2}{\Delta n_{\text{eff}} L}. \tag{12}$$

Michelson Interferometer. OFSs based on the Michelson interferometer [24, 25] are quite similar to those based on a Mach-Zehnder interferometer. The basic concept is the interference between the beams in two arms, but as each beam is reflected at the end of its arm by a mirror, only one optical fibre coupler is needed (see Fig.3). In this configuration, the light passes through both the sensing and reference arms twice, so that the FSR value is half the value of FSR_{MZI}:

$$FSR_{MI} \approx \frac{\lambda^2}{\Delta n_{\text{eff}} 2L}. \tag{13}$$

Therefore, the Michelson-based sensors intrinsically have better sensitivity. Additionally, the fact of working in reflection mode makes them more compact

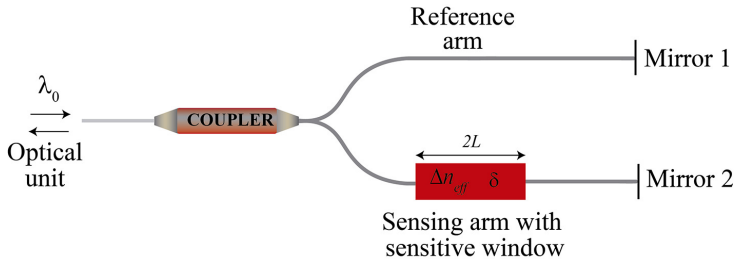

Figure 3: Schematic representation of the Michelson interferometer.

and easier to install. They also have multiplexing capabilities of multiple sensors installed in parallel. However, it is essential to adjust the fibre length difference between the reference arm and the sensing arm within the coherence length of the light source.

Sagnac Interferometer. The Sagnac Interferometer (SI) is widely used to measure rotational speed. In particular, the ring laser, which is essentially a Sagnac interferometer containing a laser in one or more of it arms, was designed specifically for that purpose. Its physical principle is based on the change in the interference fringes observed as a consequence of the different distances that the light travels due to the rotation of the observer. The simplest deduction is for a circular ring that rotates at an angular velocity ω, but the result is general for loop geometries with other shapes [17].

If a light source emits two rays in opposite directions from a point on the rotating ring, the ray traveling in the direction of rotation moves a little more than a full circumference around the ring, (see Fig.4) arriving to the start point with a delay relative to the opposite ray after a while t_1 [26]

$$t_1 = \frac{2\pi R + \Delta L}{c} \tag{14}$$

where c is the speed of the light in vacuum, R is the radius of the ring and ΔL denotes the length that the ring has rotated at this time and is calculated as follows:

$$\Delta L = R\omega t_1. \tag{15}$$

Eliminating ΔL from the two previous equations it is obtained that

$$t_1 = \frac{2\pi R}{c - R\omega}. \tag{16}$$

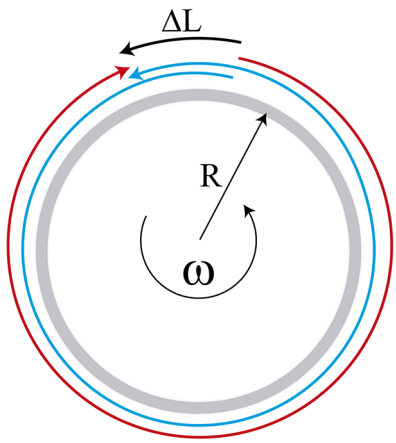

Figure 4: Figure 4: Sagnac interferometer structure

On the other hand, the light beam traveling in the opposite direction of the rotation moves slightly less than a full circumference to reach the starting point. Then, the time t_2 that the light beam needs toward in order to reach the starting point is calculated as

$$t_2 = \frac{2\pi R}{c + R\omega}. \tag{17}$$

Therefore, the time difference between the two light beams is given by

$$\Delta t = t_1 - t_2 = \frac{4\pi R^2 \omega}{c^2 - R^2\omega^2}. \tag{18}$$

If $R\omega \ll c$, then Eq.18 can be rewritten as

$$\Delta t \approx \frac{4\pi R^2 \omega}{c^2} = \frac{4A\omega}{c^2} \tag{19}$$

being A the area of the ring. Because the light beams travel different path lengths, they reach the starting point with a phase difference δ. The latter can be calculated as $\delta = 2\pi c \Delta t/\lambda$.

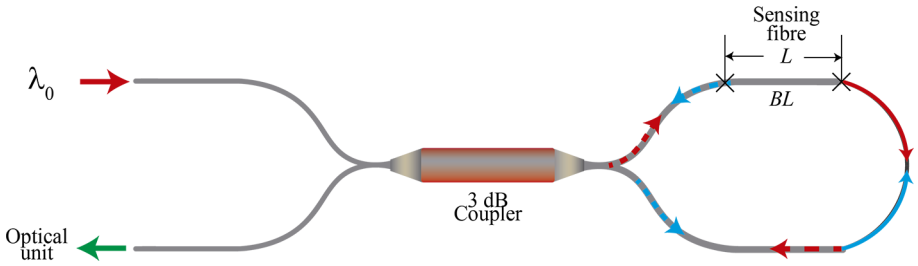

Figure 5: Sagnac-based optical fibre sensor.

In OFSs based on SI [27, 28], the Sagnac loop is made of a piece of fibre optic. As a sensing element, a high-birefringence (HiBi) fibre is normally inserted to introduce an optical path difference between the two counter-propagating waves (see Fig. 5). It causes a phase difference δ, which is calculated as

$$\delta = \frac{2\pi}{\lambda} BL \tag{20}$$

where B is the birefringence coefficient of the sensing fibre which is calculated as $B = n_f - n_s$, being n_f and n_s the effective indices of the fast and slow modes, respectively. L denotes the length of the sensing fibre. Adjusting Eq.12 to OFSs based on SIs, the free spectral range (FSR) $\Delta\lambda$ is calculated as

$$\Delta\lambda \approx \frac{\lambda^2}{BL}. \tag{21}$$

In general, FOSs based on SIs use HiBi fibres or polarization maintaining (PM) fibres as the sensing element to get a high phase sensitivity. For temperature sensing applications, the sensing fibre is doped to increase the thermal expansion coefficient, which induces high birefringence variation [29, 30]. However, for sensing other parameters such as pressure, bending or strain, the high birefringence characteristic impairs the sensing capacity due to their strong temperature dependency [31]. To overcome this problem, polarisation-maintaining photonic crystal fibres (PMPCFs) have been introduced as the sensing fibres. Photonic crystal fibres, which are made of pure silica, have low temperature dependence and their air-hole structure can be adjusted to have high birefringence [32, 33]. Furthermore, due to the asymmetry of the air hole structure, the polarisation modes are very sensitive to fibre bending, so highly sensitive

bending sensors can be fabricated based only on a photonic crystal fibre SI loop. [34]

Fabry-Perot Interferometer. In recent years the optical fibre-based Fabry-Perot resonator [35] is gaining attraction as a component suitable for spectrum analysis, laser frequency stabilization and sensing of various physical parameters of interest.

In the simplest configuration, a Fabry-Perot interferometer consists of two plane, parallel, highly reflecting surfaces, sometimes called etalon, separated by some distance d as shown in Fig 6. The enclosed air gap generally ranges from micro-metres to several centimetres when the apparatus is used interferometrically, and often to considerably greater lengths when it serves as a laser resonant cavity. If the gap can be mechanically varied by moving one of the reflecting surfaces, it is referred to as an interferometer.

In intrinsic fiber Fabry-Perot interferometric (IFPI) sensor [36, 37], mirrors are separated by a continuous segment of single-mode fibre, whereas in extrinsic Fabry-Perot interferometric (EFPI) sensors [38, 39], mirrors are separated by an air gap. These reflectors can also be formed by depositing a thin resonator cavity onto the optical fibre facet [40, 41], as illustrated in Fig.7. The FSR varies with the width of the resonator, d, which in turn varies in relation to a physical phenomenon. These changes can be calculated from Eqs. 9 and 10.

FPI-based sensors have been extensively investigated for their exceedingly effective, simple fabrication as well as low cost aspects. They have demonstrated their merit in several industrial sensing applications, including pressure, strain, acceleration, magnetic field, and temperature. Recently, these sensors have been used in some interesting applications in biology, the environment, and even in medical sciences. One of the applications is a biosensor that is capable of producing concentration-dependent signals from antibodies or antigens [42].

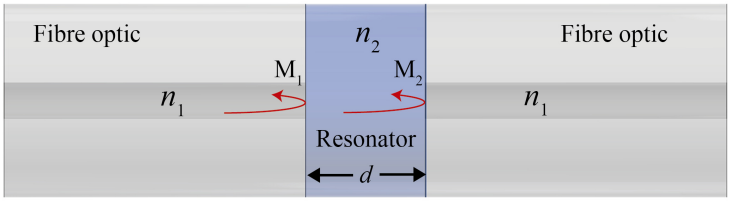

Figure 6: Schematic representation of an IFPI. M: mirror.

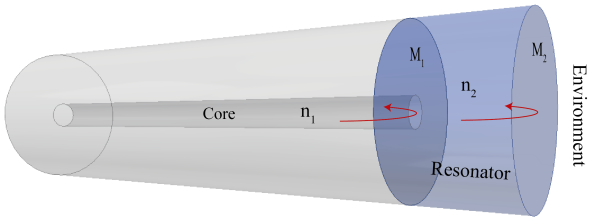

Figure 7: Schematic representation of an EFPI. M: mirror.

Such sensors also have the potential for monitoring environmental pollution or human diseases, and in the food industry.

Bragg grating-based Light Modulation. The fibre Bragg grating (FBG) sensor [43] represents the most widely studied technology for optical fibre sensors. Of the many available techniques, research has been focused on the use of FBGs as a central sensing element in the development of monitoring systems [44]. One of the main advantages of this technology is its intrinsic multiplexing capability. In fact, hundreds of fibre Bragg gratings can be written on an optical fibre, which can be as close as a few millimetres or separated by a few kilometres. With proper packaging, each of these microstructures can be made sensitive to parameters others than temperature or strain, such as, for example, pressure, acceleration, displacement, etc. This gives a multifunctional feature to the array of sensors.

An FBG is a wavelength-dependent optical filter/reflector formed by introducing a periodic refractive index structure with physical spacing $\wedge$, on the order of a wavelength of light within the core of an optical fibre as shown in Fig.8, that is to say a narrow passband filter.

When a broad-spectrum light beam is coupled in the core of an FBG (see Fig.9), reflections from each segment of alternating refractive index layers interfere constructively only for a specific wavelength of light.

This constructive reflected wavelength is called the Bragg wavelength, λ_B. The reflected light signal is a very narrow peak (width ranging from a fraction of one nanometer to a few nanometres) and is centred at the Bragg wavelength that corresponds to twice the periodic unit spacing of the gratings. This effectively causes the FBG to reflect a specific frequency of light while transmitting all others. Any change in the modal index or grating pitch of the fibre caused by

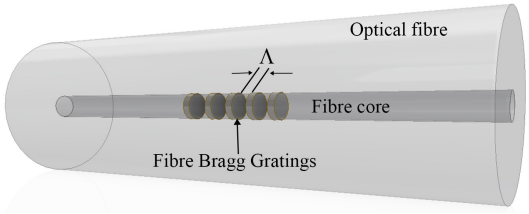

Figure 8: Illustration of a fibre Bragg grating.

strain, temperature, or polarization changes results in a Bragg wavelength shift.

λ_B is a function of the period of the microstructure ($\wedge$) and the index of refraction of the core (n_{eff}):

$$\lambda_B = 2n_{\text{eff}} \wedge . \tag{22}$$

The temperature induces changes in the refractive index of silica, as a consequence of the thermo-optic effect. There is also a contribution from the thermal expansion, which changes the period of the microstructure. It can be determined by differentiating Eq.22 [45]

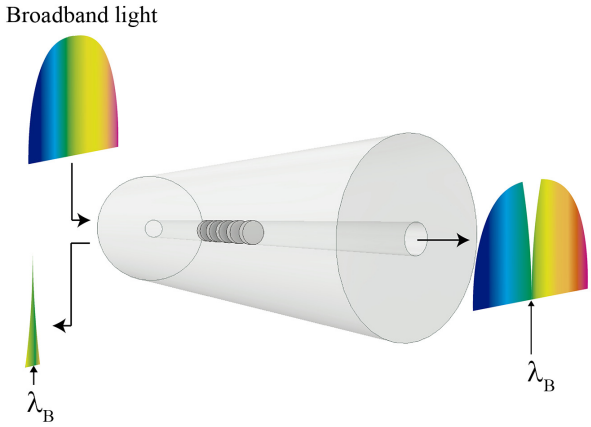

Figure 9: FBG setup

$$\frac{\Delta\lambda}{\lambda_0} = \frac{\Delta(n_{\text{eff}}\wedge)}{n_{\text{eff}}\wedge} = \left(\frac{1}{\wedge}\frac{\Delta\wedge}{\partial T} + \frac{1}{n_{\text{eff}}}\frac{\partial n_{\text{eff}}}{\partial T}\right)\Delta T. \tag{23}$$

Furthermore, when the fibre is stretched or compressed, the deformation of the optical fibre leads to a change in the period of the microstructure and, consequently, in the value of λ_B. There is also some contribution from the variation of the index of refraction through the photo-elastic effect. Similarly to the temperature, the strain dependence can be calculated as [46]

$$\frac{\Delta\lambda}{\lambda_0} = \frac{\Delta(n_{\text{eff}}\wedge)}{n_{\text{eff}}\wedge} = \left(1 + \frac{1}{n_{\text{eff}}}\frac{\partial n_{\text{eff}}}{\partial \varepsilon}\right)\Delta\varepsilon. \tag{24}$$

Distributed Optical Fibre Sensors. The concept of "distributed sensors" was first introduced in the 1980s, measuring the scattered light at every location along the fibre. There are different types of scattering, including Rayleigh, Brillouin, and Raman scattering.

Rayleigh scattering. Rayleigh is the most dominant type of scattering. It is caused by density and composition fluctuations created in the material during the manufacturing process. Rayleigh scattering is due to random variations, much smaller than the wavelength of light, in the refractive index of the fibre core. The scattered light is proportional to λ^{-4} . When a narrow pulse of light is launched into a fibre, the variation of the Rayleigh backscatter is realted to the approximate spatial location of these variations [47]. Although Rayleigh scattering is relatively insensitive to temperature, it can still be used as a distributed sensing technique for temperature and strain, and it is generally effective at distances up to 70 m. y

Brillouin scattering. Brillouin scattering is an effect caused by the third order nonlinear optical susceptibility $\chi^{(3)}$ of a medium, specifically by the part of the nonlinearity related to acoustic phonons. A photon-phonon interaction as annihilation of a pump photon, creates a Stokes photon [48] and a phonon simultaneously. The created phonon, is the vibrational modes of atoms. In silica-based optical fibres, Brillouin Stokes wave propagates dominantly backwards, although very partially, it also propagates forward. [49]. The frequency of the reflected beam, called Brillouin frequency (υ_B), corresponds to the frequency of emitted phonons which is slightly lower than that of the incident

beam. This frequency shift is stablished by a phase-matching requirement. The Brillouin shift, for pure backward Brillouin scattering, can be calculated as

$$\upsilon_b = \frac{2n_{eff}\upsilon_a}{\lambda_0} \tag{25}$$

where n_{eff} is the effective index of the propagating mode, υ_a is the acoustic velocity and λ_0 is the vacuum wavelength. This shift depends on the material composition and on the temperature and pressure of the medium. This dependence can be used for indirectly determining the influence of external or intrinsic variations in the medium where the scattering takes place. Then, Brillouin scattering of light in optical fibres can is exploited as a basis to develop accurate distributed optical sensors [50].

Raman scattering. Raman scattering is caused by the molecular vibrations of glass fibre stimulated by incident light. When monochromatic pulse light is absorbed by a molecule, it raises to a virtual excited state. The molecule may re-emit a photon of different energy, and therefore at different wavelength, either greater or smaller than the original. The energy difference will be equal to one of the vibrational/rotational energies of the molecule. Nevertheless, only if the molecule is already in an excited state at the time of photon incidence can it emit a photon of greater energy, by decaying from the excited to the ground state. This is called anti-Stokes Raman radiation and its level depends on the temperature, since the number of vibrationally/rotationally excited molecules depends directly on the absolute temperature. The emitted photons of smaller energy, decay to an excited state from an original ground state. These, are called Stokes photons. The majority of photons will be re-emitted at the same energy; it will include the Rayleigh scatter. When a high-power optical pulse, at frequency υ_i is launched into a multimode optical fibre, at a chosen value of υ, Stokes and anti-Stokes backscattered radiation levels will be at frequencies

$$\nu_s = \nu_i - \nu \tag{26}$$

$$\nu_a = \nu_i + \nu \tag{27}$$

the ratio of anti-Stokes to Stokes is given by

$$R(T) = \left(\frac{\nu_a}{\nu_s}\right)^4 exp\left(-\frac{h\nu}{kT}\right) \tag{28}$$

with the absolute temperature, T as the only unknown. The factor $(\nu_a/\nu_s)^4$ is the consequence of the Rayleigh scattering. The Raman distributed temperature sensor (RDTS) represent one of the high technology equipment for real-time measuring the spatial distribution of temperature [51, 52].

Raman scattering signals are inherently weak, especially when using visible light excitation and so a low number of scattered photons are available for detection. The signal generated by a sample can be written as

$$P_{Raman} = RN\sigma_K I \tag{29}$$

where P_{Raman} (photons/s) is the Raman power measured by the detector, R is the responsivity of the photo-detector, N is the number of the illuminated molecules, σ_K (cm2/molecule) is the Raman cross-section of the kth mode integrated over the bandwidth and over all emission directions and I (photons/cm2·s) is the incident light strikes the sample.

Raman is an intrinsically very weak phenomenon, approximately six to 10 orders of magnitude less efficient than fluorescence. However, the Raman scattering generated by molecules can be strongly amplified by placing them near the surface of suitably nanostructured substrates by means of surface-enhanced Raman scattering (SERS) technique. The latter, offers enhancement factors as high as 10^{14-15}, which are sufficient to allow even single molecule detection. Combining SERS with optical fibres can allow the monitoring of biochemical reactions in situ with high resolution. [53–55]. The latter is obviously not included as a distributed technique but as a single point sensing technique.

The next-generation sensors, then, must meet some challenging new requirements such as extreme miniaturization, ultra-low power consumption, capability to interface with networks, application-ready signal or data outputs and so on.

1.3 Hypotheses and General and Specific Aims

Optical interferometry as an accurate metrology has been widely employed in many aspects for accurate measurements of several physical quantities. As an important branch of measurement technology, nowadays the interferometry technology, based on optical fibres and laser technologies, has been highly developed and applied in sensing applications for detecting and quantifying many unknown or uncontrolled physical parameters. The optical interferometry technology is also used in the power industry for equipment failure monitoring.

Compared with the classical bulk-optic interferometer sensors, the fiber-optic interferometer sensors can achieve remote sensing and have a number of

attractive features, such as excellent sensitivity and large dynamic range, small size with rugged packages, potential for low cost, and high reliability. In general, optical fibers and fiber-optic transducers/sensors are made with totally dielectric materials that are chemically inert and completely immune to electromagnetic interference (EMI), and can also withstand relatively high temperatures. These unique properties make them very favorable to be used in harsh environments, such as inside an electric power system in which the strong EMIs often make conventional electronic sensors work unstable and result in the increase of the fault rate.

From an economic point of view, the sensors market is increasing exponentially, constituting a technology clearly of the present and of the future. Over the last few years, optical fibre sensing technology is rapidly evolving, driven mainly by telecommunication industry. Due to advantages such as spatial resolution, refresh rate, and sensing length, OFSs technology can help to progress the problem-solving capabilities of a multitude of sensor devices drawbacks. Currently, the market demands to optimise existing experimental prototypes to improve their technical limitations. In fact, the specific objectives of this thesis have been to overcome the limitations that sensor devices currently have and which are enumerated below:

1. Develop a novel technology for fabricating miniature sensor devices.
2. High sensitivity and specificity.
3. Give them the characteristic of being multipurpose.
4. Ability to sense multiple parameters simultaneously.

These goals have been achieved and demonstrated through the research manuscript presented in this thesis. The first manuscript here reported which is entitled *"Accurate microthermometer based on off center polymer caps onto optical fiber tips"*, details and demonstrates a novel fabrication technique to fabricate a micrometer-size fibre optic temperature interferometric sensor that is fast and accurate. The fabrication process is simple and reproducible. The high thermal expansion coefficient of the polymer used to build the micro-caps has allowed to achieve temperature sensitivity up to 270 pm/°C, resolution of 0.04 °C, and thermal response time of around 2.5 s. An important advantage of this device is that it operates at the well established telecommunications wavelength band. Furthermore, it has also been demonstrated that it can sense with high sensitivity, selectively and with fast response time.

This approach, with suitable polymers that can be bonded on the tip of an optical fibre, can be used to develop a myriad of microsensors for chemical or physical parameters, such as gases, pressure, etc.

In the second manuscript reported in this thesis, which is entitled "Microrefractometer Based on Off-Center Polymer Caps Bonded Onto Optical Fiber Tips", the polymer micro-cap has been evaluated as a refractometer. High-contrast (visibility) interference patterns were achieved by optimizing the size of the polymer microcaps using a fibre polishing machine. The measuring refractive index range of our devices goes from 1 up to the index of the polymer. The refractive index sensitivity was found to be higher than 10^{-4} over the whole measuring range. Temperature and refractive index cause two distinct effects on the interference patterns. Thus, our microrefractometers can be temperature self-compensated, as well.

Finally, through the manuscript reported in this thesis, entitled "*Miniature interferometric humidity sensor based on an off-center polymer cap onto optical fiber facet*" the multi-aplicability of these sensor devices have been demonstrated. To do that, several samples have been fabricated and evaluated as humidity sensors. Water molecules absorbed by the polymer microcap causes changes in the height of the microcap. This results in measurable shifts of the interference pattern. The fabricated samples were evaluated in a calibrated climatic chamber in the range from ˜10 to ˜95 % of relative humidity (RH). The sensitivity and resolution of our device was found to be 148 pm per %RH and 0.04 %RH, respectively. Thus, the technology to fabricate sensor devices here proposed can be used in a variety of practical applications that require high sensitivity, fast response, and miniature dimensions.

This approach could be suitable to fabricate sensor devices for biochemical sensing. In this type of applications, polymers permeable to chemical or biological parameters will be required. Under the presence of such parameters, the polymer refractive index can change. Such changes can be detected or monitored with the techniques demonstrated in this thesis. Furthermore, the goal of sensing different parameters simultaneously can be achieved by means of a bundle of independent sensor devices.

1.4 Summary

In summary, this thesis reports on a technology for the development of fibre-based optical sensors from a new approach.

The development of a multipurpose miniature sensor device based on an off-center polymer micro-cap bonded to the end of a single mode fibre has been

demonstrated. Its fabrication is simple and reproducible. In this device, by means of a misalignment of the micro-cap it is possible to control the fringe contrast of the interference pattern. Different samples were fabricated and experimentally tested as a temperature sensor, refractive index meter and relative humidity sensor. The sensitivities were found to be 270 pm/°C, 10^{-4} and 0.04 RH%, respectively.

The results obtained from the mentioned tests have demonstrated that in each experimental test the device behaved as fast and accurate as its commercial counterpart with which it was compared.

These devices can be useful in several applications that demand miniature sensor devices. For example, they can be useful to monitor index of liquids inside micro-fluid channels or in other small spaces. Their passive nature makes them attractive also in industrial applications. Presently, polymers with tailored optical and physical properties can be synthesized. Therefore, the performance of the sensors here proposed can be further improved. Other foreseen applications are in the field of biochemical sensing. In these applications, polymers permeable to chemical or biological parameters will be required. These parameters can be detected or monitored with the techniques reported here. In addition, the objetive of sensing different parameters simultaneously can be achieved by multiplexing a bundle of independent sensor devices.

This sensing technology could also be suitable to fabricate sensor devices to use microfluidic devices for biomarkers detection in liquid biopsies. In this type of applications, the transduction and amplification of the signal could be based on the chemical functionalisation of the polymer micro-cap onto the end-face of optical fibres. Since today polymers with tailored optical and physical properties can be synthesized, the signal transduction and amplification will be based on chemically functionalising the off-center polymer microcavity to detect only the desired target. Therefore, this approach will give practical and theoretical basis for new concepts in biosensing and will allow the design of new low cost and sensitive bioanalytical devices. Furthermore, the goal of sensing different parameters simultaneously can be achieved by means of a bundle of independent sensor devices.

To achieve high reproducibility, the manufacturing process –once the geometry of the polymer microcavity has been theoretically optimised– will be carried out automatically using opto-mechanical components controlled by an ad-hoc software created in LabVIEW. Moreover, all the components which are part of the data acquisition system (light source, coupler and interrogator) will be integrated in a device that is as small and inexpensive as possible and controlled by a user-friendly software.

1.5 References

[1] Hejun Du and Robert Bogue. Mems sensors: past, present and future. *Sensor Review*, 2007.

[2] Fulvio Vittorio Fontana. Micro-electro-mechanical systems (mems) and corresponding manufacturing process, May 2 2017. US Patent 9,642,244.

[3] Farbod Khoshnoud and Clarence W de Silva. Recent advances in mems sensor technology-mechanical applications. *IEEE Instrumentation & Measurement Magazine*, 15(2):14–24, 2012.

[4] Chris Auth, A Aliyarukunju, M Asoro, D Bergstrom, V Bhagwat, J Birdsall, N Bisnik, M Buehler, V Chikarmane, G Ding, et al. A 10nm high performance and low-power cmos technology featuring 3 rd generation finfet transistors, self-aligned quad patterning, contact over active gate and cobalt local interconnects. In *2017 IEEE International Electron Devices Meeting (IEDM)*, pages 29–1. IEEE, 2017.

[5] Heimo Uhrmann, Robert Kolm, and Horst Zimmermann. CMOS Technology. *Springer Series in Advanced Microelectronics*, 2014.

[6] *Springer Handbook of Nanotechnology.* 2010.

[7] Peter C. Schultz. *FIBER OPTICS.* 1985.

[8] E M Dianov, S L Semjonov, and I A Bufetov. New generation of optical fibres. *Quantum Electronics*, 2016.

[9] Francis Idachaba, Dike U. Ike, and Orovwode Hope. Future trends in fiber optics communication. In *Lecture Notes in Engineering and Computer Science*, 2014.

[10] Donald B. Keck. Fundamentals of Optical Waveguide Fibers. *IEEE Communications Magazine*, 1985.

[11] Alvaro A. P. Boechat, Daoning Su, D. R. Hall, and J. D. C. Jones. Bend loss in large core multimode optical fiber beam delivery systems. *Applied Optics*, 1991.

[12] Agnieszka Zuber, Malcolm Purdey, Erik Schartner, Caroline Forbes, Benjamin Van Der Hoek, David Giles, Andrew Abell, Tanya Monro, and Heike Ebendorff-Heidepriem. Detection of gold nanoparticles with different sizes using absorption and fluorescence based method. *Sensors and Actuators, B: Chemical*, 2016.

[13] Katsunari Okamoto. *Fundamentals of Optical Waveguides*. 2006.

[14] Yiping Wang, David Richardson, Gilberto Brambilla, Xian Feng, Marco Petrovich, Ming Ding, and Zhangqi Song. Intensity measurement bend sensors based on periodically tapered soft glass fibers. *Optics Letters*, 2011.

[15] Jesper B. Jensen, Lars H. Pedersen, Poul E. Hoiby, Lars B. Nielsen, T. P. Hansen, J. R. Folkenberg, J. Riishede, Danny Noordegraaf, Kristian Nielsen, A. Carlsen, and A. Bjarklev. Photonic crystal fiber based evanescent-wave sensor for detection of biomolecules in aqueous solutions. *Optics Letters*, 2004.

[16] Argha Banerjee, Sayak Mukherjee, Rishi Kumar Verma, Biman Jana, Tapan Kumar Khan, Mrinmoy Chakroborty, Rahul Das, Sandip Biswas, Ashutosh Saxena, Vandana Singh, Rakesh Mohan Hallen, Ram Swarup Rajput, Paramhans Tewari, Satyendra Kumar, Vishal Saxena, Anjan Kumar Ghosh, Joseph John, and Pinaki Gupta-Bhaya. Fiber optic sensing of liquid refractive index. *Sensors and Actuators, B: Chemical*, 2007.

[17] E Hecht. Hecht optics, 1998.

[18] Yun Jiang Rao. Recent progress in fiber-optic extrinsic Fabry-Perot interferometric sensors. *Optical Fiber Technology*, 2006.

[19] Lecheng Li, Li Xia, Zhenhai Xie, and Deming Liu. All-fiber Mach-Zehnder interferometers for sensing applications. *Optics Express*, 2012.

[20] Zhaobing Tian, Scott S.H. Yam, Jack Barnes, Wojtek Bock, Patricia Greig, James M. Fraser, Hans Peter Loock, and Richard D. Oleschuk. Refractive index sensing with Mach-Zehnder interferometer based on concatenating two single-mode fiber tapers. *IEEE Photonics Technology Letters*, 2008.

[21] B. Culshaw. The optical fibre Sagnac interferometer: An overview of its principles and applications. In *Measurement Science and Technology*, 2006.

[22] Qi Wang, Lingxin Kong, Yunli Dang, Feng Xia, Yongwei Zhang, Yong Zhao, Haifeng Hu, and Jin Li. High sensitivity refractive index sensor based on splicing points tapered SMF-PCF-SMF structure Mach-Zehnder mode interferometer. *Sensors and Actuators, B: Chemical*, 2016.

[23] Youfu Geng, Xuejin Li, Xiaoling Tan, Yuanlong Deng, and Yongqin Yu. High-sensitivity Mach-Zehnder interferometric temperature fiber sensor based on a Waist-Enlarged fusion bitaper. *IEEE Sensors Journal*, 2011.

[24] A. D. Kersey, M. J. Marrone, and M. A. Davis. Polarisation-insensitive fibre optic michelson interferometer. *Electronics Letters*, 1991.

[25] Lifeng Bao, Xinyong Dong, Perry Ping Shum, and Changyu Shen. Compact Temperature Sensor with Highly Germania-Doped Fiber-Based Michelson Interferometer. *IEEE Sensors Journal*, 2018.

[26] R. Anderson, H. R. Bilger, and G. E. Stedman. "Sagnac" effect: A century of Earth-rotated interferometers. *American Journal of Physics*, 1994.

[27] Li Yang Shao, Yuan Luo, Zhiyong Zhang, Xihua Zou, Bin Luo, Wei Pan, and Lianshan Yan. Sensitivity-enhanced temperature sensor with cascaded fiber optic Sagnac interferometers based on Vernier-effect. *Optics Communications*, 2015.

[28] Benjamin J. Vakoc, Michel J.F. Digonnet, and Gordon S. Kino. Novel fiber-optic sensor array based on the Sagnac interferometer. *Journal of Lightwave Technology*, 1999.

[29] Dae Seung Moon, Bok Hyeon Kim, Guoyong Sun, Young Geun Han, Won Taek Han, and Youngjoo Chung. The temperature sensitivity of sagnac loop interferometer based on polarization maintaining side-hole fiber. In *Optics InfoBase Conference Papers*, 2007.

[30] Ying Cui, Perry Ping Shum, Dora Juan Juan Hu, Guanghui Wang, Georges Humbert, and Xuan Quyen Dinh. Temperature sensor by using selectively filled photonic crystal fiber sagnac interferometer. *IEEE Photonics Journal*, 2012.

[31] Xinyong Dong, H. Y. Tam, and P. Shum. Temperature-insensitive strain sensor with polarization-maintaining photonic crystal fiber based Sagnac interferometer. *Applied Physics Letters*, 2007.

[32] Hyun Min Kim, Tae Hun Kim, Bongkyun Kim, and Youngjoo Chung. Temperature-insensitive torsion sensor with enhanced sensitivity by use of a highly birefringent photonic crystal fiber. *IEEE Photonics Technology Letters*, 2010.

[33] Hyun Min Kim, Tae Hun Kim, Bongkyun Kim, and Youngjoo Chung. Enhanced transverse load sensitivity by using a highly birefringent photonic crystal fiber with larger air holes on one axis. *Applied Optics*, 2010.

[34] Orlando Frazão, Josém Baptista, José L. Santos, and Philippe Roy. Curvature sensor using a highly birefringent photonic crystal fiber with two asymmetric hole regions in a Sagnac interferometer. *Applied Optics*, 2008.

[35] Norman Hodgson, Horst Weber, Norman Hodgson, and Horst Weber. The Fabry Perot Resonator. In *Optical Resonators*. 1997.

[36] T. W. Kao and H. F. Taylor. High-sensitivity intrinsic fiber-optic Fabry–Perot pressure sensor. *Optics Letters*, 1996.

[37] Daniel Jáuregui-Vázquez, Julián M. Estudillo-Ayala, Roberto Rojas-Laguna, Everardo Vargas-Rodr, Juan M. Sierra-Hernández, Juan C. Hernández-García, and Ruth I. Mata-Chávez. An all fiber intrinsic Fabry-Perot interferometer based on an air-microcavity. *Sensors (Switzerland)*, 2013.

[38] Wenhua Wang and Fang Li. Large-range liquid level sensor based on an optical fibre extrinsic Fabry-Perot interferometer. *Optics and Lasers in Engineering*, 2014.

[39] Qingxu Yu and Xinlei Zhou. Pressure sensor based on the fiber-optic extrinsic fabry-perot interferometer, 2011.

[40] Zengling Ran, Yunjiang Rao, Jian Zhang, Zhiwei Liu, and Bing Xu. A miniature fiber-optic refractive-index sensor based on laser-machined Fabry-Perot interferometer tip. *Journal of Lightwave Technology*, 2009.

[41] O. Frazão, P. Caldas, J. L. Santos, P. V. S. Marques, C. Turck, D. J. Lougnot, and O. Soppera. Fabry-Perot refractometer based on an end-of-fiber polymer tip. *Optics Letters*, 2009.

[42] L. H. Chen, C. C. Chan, R. Menon, P. Balamurali, W. C. Wong, X. M. Ang, P. B. Hu, M. Shaillender, B. Neu, P. Zu, Z. Q. Tou, C. L. Poh, and K. C.

Leong. Fabry-Perot fiber-optic immunosensor based on suspended layer-by-layer (chitosan/polystyrene sulfonate) membrane. *Sensors and Actuators, B: Chemical*, 2013.

[43] Raman Kashyap. *Fiber Bragg Gratings*. 2010.

[44] Mousumi Majumder, Tarun Kumar Gangopadhyay, Ashim Kumar Chakraborty, Kamal Dasgupta, and D. K. Bhattacharya. Fibre Bragg gratings in structural health monitoring-Present status and applications, 2008.

[45] Elton Soares de Lima Filho, Mohamad Diaa Baiad, Mathieu Gagné, and Raman Kashyap. Fiber Bragg gratings for low-temperature measurement. *Optics Express*, 2014.

[46] Carlo Edoardo Campanella, Antonello Cuccovillo, Clarissa Campanella, Abdulkadir Yurt, and Vittorio M.N. Passaro. Fibre Bragg Grating based strain sensors: Review of technology and applications, 2018.

[47] Richard B. Miles, Walter R. Lempert, and Joseph N. Forkey. Laser Rayleigh scattering. *Measurement Science and Technology*, 2001.

[48] J. R. Albani. *Structure and Dynamics of Macromolecules: Absorption and Fluorescence Studies*. 2004.

[49] Weiwen Zou, Xin Long, and Jianping Chen. Brillouin Scattering in Optical Fibers and Its Application to Distributed Sensors. In *Advances in Optical Fiber Technology: Fundamental Optical Phenomena and Applications*. 2015.

[50] C. A. Galindez-Jamioy and J. M. López-Higuera. Brillouin distributed fiber sensors: An overview and applications, 2012.

[51] M. C. Farries and A. J. Rogers. Distributed Sensing Using Stimulated Raman Interaction In A Monomode Optical Fibre. In *2nd Intl Conf on Optical Fiber Sensors: OFS'84*, 1984.

[52] Iacopo Toccafondo, Tiziano Nannipieri, Alessandro Signorini, Elisa Guillermain, Jochen Kuhnhenn, Markus Brugger, and Fabrizio Di Pasquale. Raman Distributed Temperature Sensing at CERN. *IEEE Photonics Technology Letters*, 2015.

[53] Tanya Hutter, Stephen R. Elliott, and Sumeet Mahajan. Optical fibre-tip probes for SERS: numerical study for design considerations. *Optics Express*, 2018.

[54] P. R. Stoddart and D. J. White. Optical fibre SERS sensors, 2009.

[55] Job M. Bello, V. Anantha Narayanan, David L. Stokes, and Tuan Vo-Dinh. Fiber-Optic Remote Sensor for in Situ Surface-Enhanced Raman Scattering Analysis. *Analytical Chemistry*, 1990.

2 Conclusions

This thesis has reported on the development of a novel sensing technology based on optical fibre to fabricate miniature sensor devices. The fabrication of our devices is simple and reproducible. An important advantage of these devices is that they operate at the well-established telecommunications wavelength bands. Different samples have been experimentally tested as a temperature sensor, refractive index meter and RH sensor. The results obtained from the mentioned tests have shown that in each experimental test our device behaved as fast and accurate as its commercial counterpart with which it was compared. Another advantage is that our device can operate in a broad wavelength range (from 800 to 1600 nm, approximately).

By means of this technology, it is possible to control the coupling coefficient and thus, the reflection of the interface between the polymer and the external medium, allowing to optimize the fringe contrast of the interference pattern. The theoretical knowledge of the mode coupling coefficient, here developed and demonstrated, makes this approach applicable not only to the applications reported here, but to many others as well. Its micro-size makes it suitable to be useful in several applications that demand miniature sensors. The devices here proposed can be useful in miniature spaces where reliable and accurate humidity measurements are needed. Other applications that we foresee are in the field of bio-chemical sensing. In these applications, synthesized polymers with tailored optical and physical properties will be required. Then, under the presence of the parameters to sense, the interference pattern will change, and therefore will be detected or monitored with the techniques proposed in this thesis.

The author considers that this new approach could be the key to the fabrication of new fibre-based sensing devices with more capabilities and better features than previously have been achieved. Therefore, the goal of the thesis has been accomplished. However, there are improvements in which the author will continue to work on to give to the devices greater potential. It is important to note that the technologies presented here, open the way for manufacturing sensor devices with much-needed capabilities and features that are in demand in leading and emerging industries.

3 Appendix

Sensors & Actuators: B. Chemical 272 (2018) 612–617

Contents lists available at ScienceDirect

Sensors and Actuators B: Chemical

journal homepage: www.elsevier.com/locate/snb

Accurate microthermometer based on off center polymer caps onto optical fiber tips

Oskar Arrizabalaga[a], Gaizka Durana[a], Joseba Zubia[a], Joel Villatoro[a,b,*]

[a] Department of Communications Engineering, Escuela de Ingenieria de Bilbao, University of the Basque Country (UPV/EHU), Plaza Ingeniero Torres Quevedo 1, E-48013 Bilbao, Spain

[b] IKERBASQUE–Basque Foundation for Science, E-48011 Bilbao, Spain

ARTICLE INFO

Keywords:
Optical fiber sensors
Fabry-Perot interferometers
Polymer cavity
Temperature sensors
Microsensors

ABSTRACT

We report on microscopic polymer spherical caps bonded onto the cleaved end of a single-mode fiber (SMF) for fast, accurate, and sensitive temperature sensing. The microcaps were fabricated by dispensing sub nano-liter amounts of UV-curable polymer onto the end face of a standard SMF that was cleaved at a small angle. A reflection from the SMF-polymer interface combined with a reflection from the polymer-external medium interface gives rise to a well-defined interference pattern. The high thermal expansion coefficient of the polymer used to build the micro-caps allowed us to achieve temperature sensitivity up to 270 pm/°C, resolution of 0.04 °C, and thermal response time of around 2.5 s. The simple fabrication process and the broad operating wavelength (from 800 to 1600 nm, approximately) of our devices along with the diversity of polymers currently available, make the concept and approach proposed here appealing for diverse sensing applications.

1. Introduction

As part of safety and quality control in industrial production, temperature is a crucial parameter that must be monitored or controlled. In environmental and bio-medical applications, temperature is also a parameter that is monitored constantly. As optical fiber temperature sensors (or thermometers) are capable of operating, hence to gather data, in environments where electromagnetic, radio frequency, or microwave radiation is present, they have gained considerable attention in the industrial and bio-medical sectors.

The fiber optic sensor community has exploited different methods and techniques to devise point optical fiber thermometers that include mode interferometers [1–4] and long period gratings (LPG) [5–8]. Such temperature sensors are robust and highly sensitive but their response time is slow, typically of several seconds. Moreover, in most cases, the sensitive segment of such thermometers is several millimeters, and even of centimeters, long. This makes them unsuitable for applications where space is small. To the authors' best knowledge, point thermometers based on mode interferometers or LPGs have not reached commercial level yet.

Other fiber optic temperature sensors reported so far are based on Fabry-Perot interferometry. The cavity, i.e., the sensitive element of the interferometers, can be made with a short segment of glass [9–11], polymer [12–15], or silicon [16,17]. These types of sensors are compact and highly sensitive. However, elaborated or multistep fabrication processes are required to achieve highly uniform cavities, hence high performance Fabry-Perot interferometers or thermometers.

To the authors' best knowledge, the most accurate fiber optic thermometers exploit the temperature dependence of fiber Bragg gratings (FBGs) [18–23], fluorescent materials [24–29], or GaAs semiconductor crystals [30,31]. The level of maturity of such techniques is high to a point that they have reached commercial level [32]. The main characteristics of thermometers based on FBGs include a sensitive segment of several millimeters in length (the length of the grating); thermal response time of several seconds, and temperature sensitivity of around 10 pm/°C [18–23]. FBG thermometers tend to be expensive as their interrogation requires a pico-meter resolution detection system. On the other hand, thermometers based on fluorescent materials or semiconductor crystals are characterized by a fast response time, a sensitive material of few hundred micrometers in length or diameter attached to the end of a multimode optical fiber. The assembly of thermometers based on the aforementioned materials is complex. In addition, they can operate in short distances (a few tens of meters) as the fluorescent signal is low because they operate in non-telecommunications wavelengths.

As an alternative to the fiber optic thermometers discussed above, in

* Corresponding author at: Department of Communications Engineering, Escuela de Ingenieria de Bilbao, University of the Basque Country (UPV/EHU), Plaza Ingeniero Torres Quevedo 1, E-48013 Bilbao, Spain.
E-mail address: agustinjoel.villatoro@ehu.eus (J. Villatoro).

https://doi.org/10.1016/j.snb.2018.05.148
Received 10 January 2018; Received in revised form 24 May 2018; Accepted 25 May 2018
Available online 26 May 2018
0925-4005/

this paper we propose an accurate interferometric thermometer that has the following remarkable features: *i*) microscopic dimensions, *ii*) simple fabrication and interrogation, and *iii*) operation over a wide wavelength range, from 800 to 1600 nm, approximately. Our device can sense temperature from –25 to 125 °C with high sensitivity (up to 270 pm/°C) and fast response time (2.5 s). The sensitive section of our micro-thermometer is made of a UV curable polymer that is deposited onto the end face of a single mode fiber (SMF) that is cleaved at a small angle. As a result, an off center spherical microcap is formed. Light reflected from the SMF-polymer interface is combined with that reflected from the polymer-external-medium interface. Due to the asymmetry of the two reflecting surfaces, the interference pattern exhibits a well-defined series of maxima and minima. We found that our sensors are as accurate as commercial electronic thermometers. Thus, we believe that the temperature sensors here proposed can be used in a variety of practical applications that require high sensitivity, fast thermal response, and miniature dimensions.

2. Sensor fabrication and operation principle

Our device consists of a microscopic polymer spherical cap formed on the end face of a standard single mode fiber (SMF) which is cleaved at a small angle. It is depicted in Fig. 1(a). The experimental set-up used to create such a microscopic spherical cap is shown schematically in Fig. 1(b). The fabrication steps are as follows. Firstly, two SMFs are cleaved with a conventional fiber optic cleaver. In our case, we used a cleaver from Fujikura, model CT-32. The typical cleave angle, i.e., the most probably angle, that is achieved with such a cleaver is ~0.5°. The cleaved optical fibers were cleaned with alcohol in an ultrasonic cleaner, and then they were clamped in separate 3-axis optical fiber alignment stages (ULTRAlign™, Newport). In our arrangement, the SMFs were placed in vertical position for the reasons explained below. One of the SMFs was the sensing fiber and the other one was used as a dispensing fiber. Our set up had also a CMOS USB camera to monitor the deposition of the polymer on the SMF face. To optimize the alignment between the SMFs, as well as to monitor the interference pattern of the samples, light from a super luminescent diode (SLD) was launched to the sensing SMF; the reflected light was sent to a mini-spectrometer by means of a suitable optical fiber coupler, see Fig. 1(b). The interference patterns were observed, stored, and analyzed, in a personal computer.

The dispensing SMF was dipped into a liquid polymer and then, it was gently withdrawn. The polymer we used is commercially known as NOA81 (from Norland Products Inc.). We used such polymer because it is cured in seconds and has excellent adhesion to glass. However, other polymers that can be bounded to glass can be used. After withdrawing the dispensing fiber from the liquid polymer, the fiber tip and the sides were coated with polymer, see the photograph shown in Fig. 1(c). The polymer-coated SMF was placed beneath, and in close proximity, to the sensing SMF. Immediately after that, the fibers were aligned with the 3-axis stages. The alignment between the SMFs was stopped when a well defined interference pattern was observed. Such an interference pattern was due to an air cavity formed between the facet of the sensing SMF and the liquid polymer covering the dispensing SMF. Afterwards, the polymer-coated SMF was moved towards the sensing SMF until the polymer touched the end face of the sensing SMF, see Fig. 1(d). The dispensing SMF was then displaced far away from the sensing SMF; see Fig. 1(e).

It can be noted from the photograph that, due to surface tension, a microscopic polymer spherical cap is formed only onto the end face of the sensing SMF. The small angle of the SMF face makes the polymer microcap to be off center. In the final step of the fabrication process, the polymer was cured by illuminating it with UV light, with peak emission at 365 nm (CS2010, UV Curing LED System from Thorlabs), during 30 s. Under these conditions, the polymer spherical microcap becomes solid, and it is strongly bonded to the SMF. As recommended by the polymer manufacturer, for an optimum adhesion, the microcap was aged at 50 °C during 12 h. If other polymers are used, probably such an aging process is not necessary.

The interference patterns of our devices were analyzed after the fabrication process. The samples were also inspected under an optical microscope. After a single deposition process, d was found to be ~20 μm. This suggests that the volume of the spherical microcap, or the volume of polymer deposited on the SMF facet was on the order of ~0.15 nano-liters.

The operating principle of our sensor is explained as follows. Let us assume that a wave with amplitude E_0 propagates without attenuation in the core of the SMF, see Fig. 1(a). When such a wave reaches the SMF-polymer interface, it is partially reflected, the rest is transmitted to the polymer. The amplitude of the reflected wave (E_{r1}) can be expressed

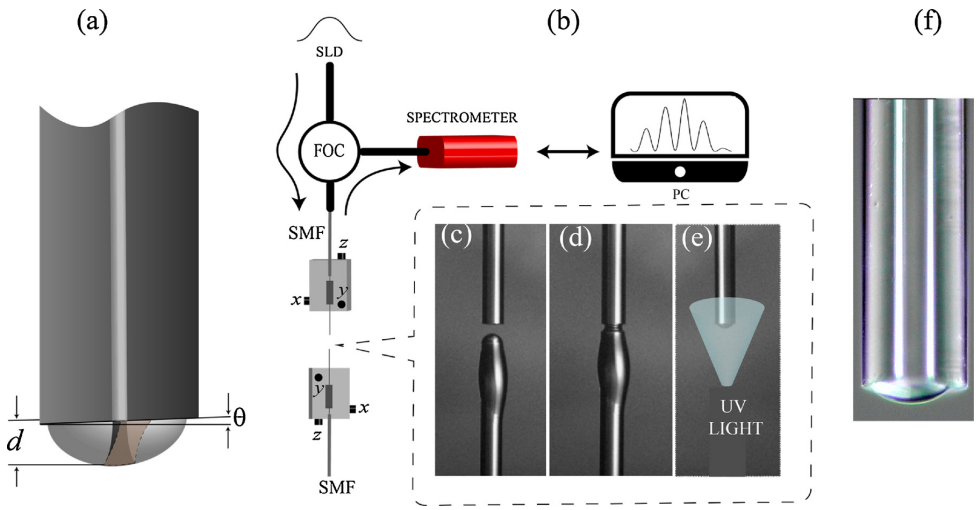

Fig. 1. (a) Illustration of the temperature microsensor, d is the height of polymer microcap and θ the fiber cleave angle. (b) Schematic representation of the set-up used to monitor the fabrication process and to interrogate the devices. (c), (d) and (e) Sensor fabrication steps. SLD is superluminescent diode, SMF, single mode fiber, FOC, fiber optic coupler, and PC, personal computer. (f) Micrograph of an as-fabricated sample where d was 20 μm.

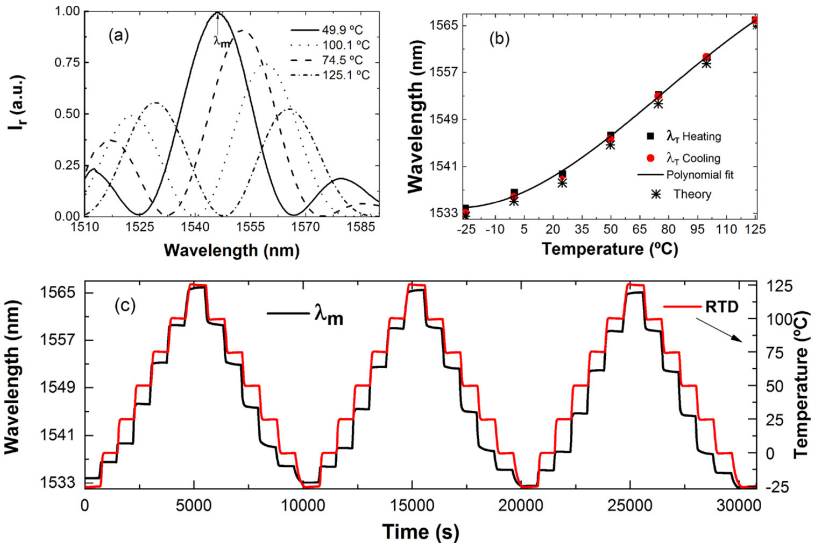

Fig. 2. (a) Spectra of the temperature sensor at different temperatures. λ_m is the maximum of each spectrum. (b) Plot of λ_m versus temperature; the asterisks show the theoretical value of λ_m vs temperature and the squares and dots are experimental values. (c) Comparative of our temperature sensor with a commercial thermometer during several temperature cycles in steps of ~25 °C.

as:

$$E_{r1} = r_1 E_0, \tag{1}$$

where r_1 is the amplitude reflection coefficient which depends on the refractive indices of the polymer (n_p) and the fiber core (n_c), as $r_1 \approx (n_p - n_c)/(n_p + n_c)$. It is important to point out that the expression for r_1 is valid for quasi-perpendicular incidence and random polarized light. The wave that propagates in the polymer reaches the polymer-external-medium interface with an accumulated phase of $\phi = 2\pi n_p d/\lambda$, with d is the height of the polymer microcap and λ is the wavelength of the optical source. Such a wave suffers Fresnel reflection from the polymer-external-medium interface if the index of the polymer, n_p, and the refractive index of the external medium (n_e) are different.

The amplitude of the reflected wave (E_{r2}) can be expressed as $E_{r2} = E_0 r_2(1\text{-}r_1)exp(\text{-}i\phi)$ where r_2 is the amplitude reflection coefficient which is expressed as $r_2 \approx (n_e - n_p)/(n_e + n_p)$. In our experiments, the external medium was air ($n_e = 1$). In our devices, not all the reflected wave from the polymer-external medium interface is coupled into the SMF core. Due to the small angle of the SMF face, the fiber facet and the curved surface of the polymer microcap are not parallel. That is the reason we do not treat our devices as a Fabry-Perot interferometer.

The reflected wave that is coupled back to the SMF core be expressed as:

$$E_c = \eta r_2 E_0 (1 - r_1)^2 \exp(-i2\phi). \tag{2}$$

In Eq. (2), η is the coupling coefficient that can be calculated from Eqs. A7 and A8 given in Ref. [33]. According to the latter reference, η depends on the angle of the SMF face, d, n_p, λ, spot size of the output beam of the SMF, etc.

The amplitude of the total reflected field (E_T) is the sum of E_{r1} and E_c:

$$E_T = E_0[r_1 + \eta r_2(1 - r_1)^2 \exp(-i2\phi)]. \tag{3}$$

Thus, the total reflected intensity that can be measured is $(E_T)^2$. By defining $I_r = (E_T/E_0)^2$ we get

$$I_r = r_1^2 + \eta^2 r_2^2 (1 - r_1)^4 + 2\eta r_1 r_2 (1 - r_1)^2 \cos(2\phi). \tag{4}$$

From Eq. (4), it can be deduced that I_r will be maximum when $\phi = 2m\pi$ and minimum when $\phi = (2m + 1)\pi$, m being a positive integer. Thus, the peaks of the interference pattern (maximum values of I_r) are found at wavelengths that satisfy the condition:

$$\lambda_m = (2n_p d)/m. \tag{5}$$

Note also from Eqs. (4) and (5) that η, that depends on the cleaved angle of the SMF, d, n_p, etc., will affect only on the contrast (or visibility) of the interference pattern but not the position of the maxima.

The temperature effect on our devices can be obtained by differentiating Eq. (5) with respect to temperature (T). We obtain:

$$\frac{\partial \lambda_m}{\partial T} = \left[\frac{1}{n_p}\frac{\partial n_p}{\partial T} + \frac{1}{d}\frac{\partial d}{\partial T}\right]\lambda_m. \tag{6}$$

The terms, $\partial n_p/\partial T$ and $\partial d/\partial T$, in Eq. (6) are, respectively, the thermo-optic coefficient (TOC) and the thermal expansion coefficient (TEC) of the material the microcap is made of. The refractive index of the polymer depends also on the wavelength of the optical source. According to the manufacturer, for the case of the NOA81 polymer, $n_p = A + B/\lambda^2 + C/\lambda^4$, with $A = 1.5375$, $B = 8290.45$, and $C = -2.11046 \times 10^8$; the TOC value is -1.83×10^{-4}/°C and the TEC value is 2.4×10^{-4}/°C.

From Eqs. (5) and (6), it can be concluded that the position of λ_m (a parameter that is easy to monitor) and the thermal sensitivity depend only on the TEC and TOC of the polymer used to fabricate the microcap. As the TEC value is higher that the TOC value of the NOA81 polymer, λ_m will shift to longer wavelengths when temperature increases. It should be pointed out that if other polymer is used to fabricate the sensor where the TOC be higher than the TEC, the shift of the interference pattern will be to shorter wavelengths when temperature increases. Regardless the direction of the shift, temperature will be codified in wavelength, an absolute parameter, similar to FBG-based or semiconductor-based temperature sensors [18–23,30,31].

3. Experimental results and discussion

To evaluate our devices as temperature sensors, they were first encapsulated with miniature stainless steel tubes (from Omega Solutions Inc.). Then, they were placed inside a temperature calibrator (LTR-25/140, from Kaye) that operates from −25 °C to 140 °C. However, according to the manufacturer, the NOA81 polymer, once cured and aged, can withstand temperatures from −150 °C to 125 °C. Thus, the calibration was carried out from −25 to +125 °C.

As a reference, a precision and calibrated commercial RTD -resistance temperature detector- (Pt100 HH804U from Omega®) was

placed inside the temperature calibrator, together with our devices. The interrogation of our devices was carried out with the components described in Fig. 1.

In Fig. 2(a), we show the observed spectra at different temperatures of a sample with a polymer cap where $d \sim 20\,\mu m$. The red shift of the interference pattern is evident. The calibration curve is shown in Fig. 2(b). The theoretical fitting was carried out by considering a coupling factor $\eta = 0.18$. It can be seen that the device does not show any hysteresis. From Fig. 2 we calculated the relationship between λ_m and T as

$$\lambda_m(nm) = 1535.99 + T\cdot(0.13 + 0.001\cdot T - 7.96\cdot 10^{-6}\cdot T^2) \quad (7)$$

From the calibration curve, the temperature sensitivity in the linear range, i.e., from 15 °C to 125 °C, was found to be 270 pm/°C. Such sensitivity is an order of magnitude higher than that of FBG temperature sensors. With our interrogation system, the position of λ_m could be monitor with 10 pm precision. This means that our microthermometers can reach a resolution of 0.04 °C.

An additional test to our samples consisted in exposing them repeatedly to several temperature cycles during more than 8 h. The temperature was increased from −25 °C to +125 °C in steps of 25 °C. Then, the temperature was decreased from +125 °C to −25 °C in steps of 25 °C. The results of our experiments are shown in Fig. 2(c). From the figure, it can be seen that our devices are as accurate as a commercial RTD.

Another test that we carried out consisted in the assessment of the response of our devices to temperature pulses, from 20 to 70 °C. Such a temperature range was chosen because it is the range of interest in biomedical applications. In Fig. 3(a) we show the results of our experiments. Again, we can see that our sensor provides accurate information as an RTD but the results suggest that our microthermometers respond faster than an RTD.

The response time of our devices was experimentally measured. For that, a microthermometer was encapsulated with a short segment of silica capillary of 150 µm and 300 µm of inner and outer diameter, respectively. Our device was attached to an RTD, and then, they were immersed in hot water. The temperature of the hot water was monitored with the RTD. The temperature of the external environment was monitored with another RTD. Fig. 3(b) shows the wavelength shift of our device under study as a function of time when the temperature increased from 24 to 37.9 °C. From the figure, we calculated the thermal response time of our device. It was found to be 2.5 s. Such a response time is faster than that of other fiber optic temperature sensors, as for example, FBG-based thermometers.

We also fabricated and characterized some samples that operated at shorter wavelengths. To do so, we used an SMF at 850 nm (HP780, from Thorlabs). The deposition of the microcaps was carried out with the same steps described above. The height of the microcap was again ~20 µm. At shorter wavelengths, the refractive index of the polymer is higher. The combination of shorter wavelengths and higher index makes the period of the interference pattern larger at 850 nm. Fig. 4(a) shows the output spectra of the quoted device at different temperatures. Again, a shift to longer wavelengths as the temperature increased was found. The calibration curve is shown in Fig. 4(b). Note the linear dependence of λ_m on temperature in the range from 15 to 125 °C. In that range, the temperature sensitivity was found to be 210 pm/°C. This suggests that there is no loss of temperature sensitivity at shorter wavelengths.

We also exposed the samples repeatedly to several temperature cycles during 10 h approximately. The temperature was increased from −25 °C to +125 °C; and then it was decreased to −25 °C. The steps were also 25 °C. The results of our experiments are shown in Fig. 4(c). It can be noted from such a figure that our devices provide information of temperature as a well-calibrated RTD. An advantage of fiber optic thermometers that operate at 850 nm is the fact that light sources and spectrometers are less expensive. Hence, cost effective microthermometers can be developed.

4. Conclusions

We have reported on micrometer-size fiber optic temperature interferometric sensors that are fast and accurate. The fabrication of our devices is simple and reproducible. An important advantage of our devices is that they operate at the well-established telecommunications wavelength bands. In our devices, the temperature sensitive region is a microscopic polymer spherical cap bonded onto the facet of a single mode optical fiber, which is cleaved at a small angle. Our devices have high temperature sensitivity and resolution and respond fast to temperature changes.

The performance of the sensors here proposed can be further improved. The science and technology of polymers is mature. Currently, polymers with tailored optical and physical properties can be synthesized. This may allow to tailor the thermal response time, temperature sensitivity, or operating temperature range of our devices.

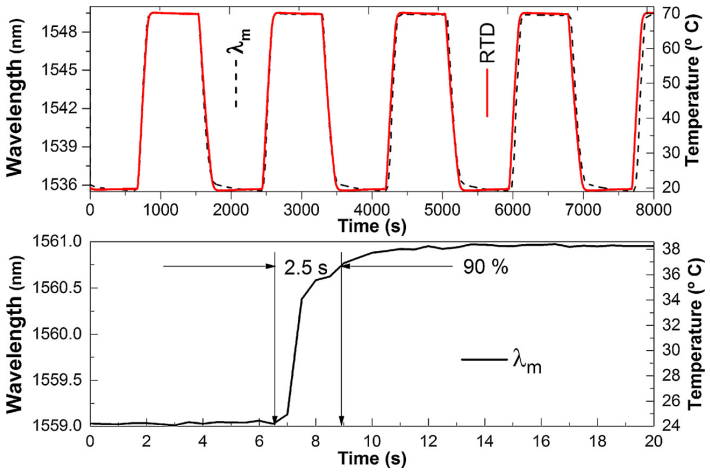

Fig. 3. (a) Comparative between our sensor and the RTD of temperature pulses in the range of interest in medical applications. (b) Response time of the temperature sensor.

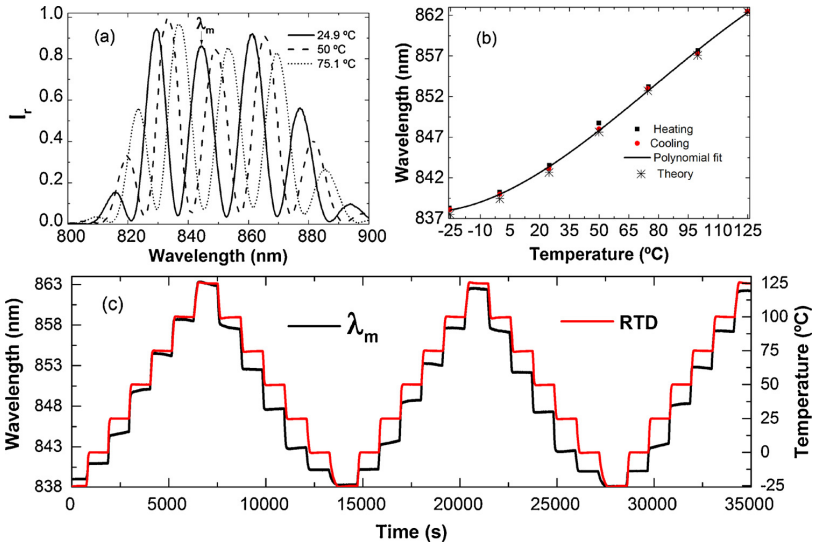

Fig. 4. (a) Spectra at around 850 nm at different temperatures of a sample where the polymer microcap had a $d = 20\,\mu m$. (b) Experimental and theoretical values (asteriks) of λ_m as a function of temperature. (c) Comparative of our temperature sensor with a commercial thermometer during several temperature cycles in steps of 25°.

We believe that the devices here proposed can be useful in several applications that demand miniature thermometers. For example, they can useful to explore temperature inside micro-fluid channels or other small spaces or to monitor temperature of tiny objects. Their fast thermal response time makes them attractive to monitor temperature in environmental or biomedical applications. Due to their passive nature, the microthermometers reported here can be attractive in industrial applications.

Acknowledgements

This work has been funded in part by the Fondo Europeo de Desarrollo Regional (FEDER); by the Ministerio de Economía y Competitividad [TEC2015-638263-C03-1-R]; by the Gobierno Vasco/Eusko Jaurlaritza [IT933-16]; and ELKARTEK [KK-2016/0030, KK-2017/00033, KK-2017/00089 and KK-2016/0059]. Oskar Arrizabalaga acknowledges a PhD fellowship from the Departamento de Educación, Política Lingüística y Cultura del Gobierno Vasco/Eusko Jaurlaritza.

References

[1] W. Eickhoff, Temperature sensing by mode–mode interference in birefringent optical fibers, Opt. Lett. 6 (1981) 204–206, http://dx.doi.org/10.1364/OL.6.000204.
[2] E. Li, X. Wang, C. Zhang, Fiber-optic temperature sensor based on interference of selective higher-order modes, Appl. Phys. Lett. 89 (2006) 091119, , http://dx.doi.org/10.1063/1.2344835.
[3] J.E. Antonio-Lopez, Z.S. Eznaveh, P. LiKamWa, A. Schülzgen, R. Amezcua-Correa, Multicore fiber sensor for high-temperature applications up to 1000 °C, Opt. Lett. 39 (2014) 4309–4312, http://dx.doi.org/10.1364/OL.39.004309.
[4] I. Hernandez-Romano, D. Monzon-Hernandez, C. Moreno-Hernandez, J. Moreno-Hernandez, Highly sensitive temperature sensor based on a polymer-coated microfiber interferometer, IEEE Photonics Technol. Lett. 27 (2015) 2591–2594, http://dx.doi.org/10.1109/LPT.2015.2478790.
[5] V. Bhatia, A.M. Vengsarkar, Optical fiber long-period grating sensors, Opt. Lett. 21 (1996) 692–694, http://dx.doi.org/10.1364/OL.21.000692.
[6] S. Khaliq, S.W. James, R.P. Tatam, Enhanced sensitivity fibre optic long period grating temperature sensor, Meas. Sci. Technol. 13 (2002) 792–795, http://dx.doi.org/10.1088/0957-0233/13/5/318.
[7] S.K. Abi Kaed Bey, T. Sun, K.T.V. Grattan, Optimization of a long-period grating-based Mach-Zehnder interferometer for temperature measurement, Opt. Commun. 272 (2007) 15–21, http://dx.doi.org/10.1016/j.optcom.2006.11.016.
[8] C. Du, Q. Wang, Y. Zhao, J. Li, Highly sensitive temperature sensor based on an isopropanol-filled photonic crystal fiber long period grating, Opt. Fiber Technol. 34 (2017) 12–15, http://dx.doi.org/10.1016/j.yofte.2016.11.013.
[9] C.E. Lee, H.F. Taylor, Fiber-optic Fabry-Perot temperature sensor using a low-coherence light source, J. Light. Technol. 9 (1991) 129–134, http://dx.doi.org/10.1109/50.64932.
[10] H.Y. Choi, K.S. Park, S.J. Park, U.C. Paek, B.H. Lee, E.S. Choi, Miniature fiber-optic high temperature sensor based on a hybrid structured Fabry-Perot interferometer, Opt. Lett. 33 (2008) 2455–2457, http://dx.doi.org/10.1364/OL.33.002455.
[11] S. Pevec, D. Donlagic, High resolution, all-fiber, micro-machined sensor for simultaneous measurement of refractive index and temperature, Opt. Express 22 (2014) 16241–16253, http://dx.doi.org/10.1364/OE.22.016241.
[12] X.L. Tan, Y.F. Geng, X.J. Li, Y.L. Deng, Z. Yin, R. Gao, UV-curable polymer microhemisphere-based fiber-optic Fabry-Perot interferometer for simultaneous measurement of refractive index and temperature, IEEE Photonics J. 6 (2014) 7800208, , http://dx.doi.org/10.1109/JPHOT.2014.2332460.
[13] B. Sun, Y. Wang, J. Qu, C. Liao, G. Yin, J. He, J. Zhou, J. Tang, S. Liu, Z. Li, Y. Liu, Simultaneous measurement of pressure and temperature by employing Fabry-Perot interferometer based on pendant polymer droplet, Opt. Express 23 (2015) 1906–1911.
[14] M. Li, Y. Liu, R. Gao, Y. Li, X. Zhao, S. Qu, Ultracompact fiber sensor tip based on liquid polymer-filled Fabry-Perot cavity with high temperature sensitivity, Sens. Actuators B Chem. 233 (2016) 496–501, http://dx.doi.org/10.1016/j.snb.2016.04.121.
[15] I. Hernández-Romano, M.A. Cruz-Garcia, C. Moreno-Hernández, D. Monzón-Hernández, E.O. López-Figueroa, O.E. Paredes-Gallardo, M. Torres-Cisneros, J. Villatoro, Optical fiber temperature sensor based on a microcavity with polymer overlay, Opt. Express. 24 (2016) 5654–5661, http://dx.doi.org/10.1364/OE.24.005654.
[16] G. Liu, M. Han, W. Hou, High-resolution and fast-response fiber-optic temperature sensor using silicon Fabry-Pérot cavity, Opt. Express 23 (2015) 7237–7247, http://dx.doi.org/10.1364/OE.23.007237.
[17] G. Liu, Q. Sheng, W. Hou, M. Han, High-resolution, large dynamic range fiber-optic thermometer with cascaded Fabry–Perot cavities, Opt. Lett. 41 (2016) 5134–5137.
[18] A.D. Kersey, T.A. Berkoff, Fiber-optic bragg-grating differential-temperature sensor, IEEE Photonics Technol. Lett. 4 (1992) 1183–1185, http://dx.doi.org/10.1109/68.163773.
[19] Y.J. Rao, D.J. Webb, D.A. Jackson, L. Zhang, I. Bennion, In-fiber Bragg-grating temperature sensor system for medical applications, J. Lightw. Technol. 15 (1997) 779–784, http://dx.doi.org/10.1109/50.580812.
[20] D. Grobnic, S.J. Mihailov, C.W. Smelser, H. Ding, Sapphire fiber Bragg grating sensor made using femtosecond laser radiation for ultrahigh temperature applications, IEEE Photon. Technol. Lett. 16 (2004) 2505–2507, http://dx.doi.org/10.1109/LPT.2004.834920.
[21] B. Zhang, M. Kahrizi, High-temperature resistance fiber Bragg grating temperature sensor fabrication, IEEE Sens. J. 7 (2007) 586–591, http://dx.doi.org/10.1109/JSEN.2007.891941.
[22] Y. Zhan, S. Xue, Q. Yang, S. Xiang, H. He, R. Zhu, A novel fiber Bragg grating high-temperature sensor, Optik 119 (2008) 535–539, http://dx.doi.org/10.1016/j.ijleo.2007.02.010.
[23] D. Barrera, V. Finazzi, J. Villatoro, S. Sales, V. Pruneri, Packaged optical sensors based on regenerated fiber Bragg gratings for high temperature applications, IEEE Sens. J. 12 (2012) 107–112, http://dx.doi.org/10.1109/JSEN.2011.2122254.
[24] H. Berthou, C.K. Jörgensen, Optical-fiber temperature sensor based on upconversion-excited fluorescence, Opt. Lett. 15 (1990) 1100–1102, http://dx.doi.org/10.1364/OL.15.001100.
[25] S.A. Wade, S.F. Collins, G.W. Baxter, Fluorescence intensity ratio technique for optical fiber point temperature sensing, J. Appl. Phys. 94 (2003) 4743–4756, http://dx.doi.org/10.1063/1.1606526.

[26] S.A. Wade, S.F. Collins, G.W. Baxter, Fluorescence intensity ratio technique for optical fiber point temperature sensing, J. Appl. Phys. 94 (2003) 4743–4756, http://dx.doi.org/10.1063/1.1606526.
[27] S. Baek, Y. Jeong, J. Nilsson, J.K. Sahu, B. Lee, Temperature-dependent fluorescence characteristics of an ytterbium-sensitized erbium-doped silica fiber for sensor applications, Opt. Fiber Technol. 12 (2006) 10–19, http://dx.doi.org/10.1016/j.yofte.2005.04.002.
[28] S. Musolino, E.P. Schartner, G. Tsiminis, A. Salem, T.M. Monro, M.R. Hutchinson, Portable optical fiber probe for in vivo brain temperature measurements, Biomed. Opt. Express. 7 (2016) 3069–3077, http://dx.doi.org/10.1364/BOE.7.003069.
[29] Y. Zhao, M.Q. Chen, R.Q. Lv, P. Wang, X. Feng, Small and practical optical fiber fluorescence temperature sensor, IEEE Trans. Instrum. Meas. 65 (2016) 2406–2411, http://dx.doi.org/10.1109/TIM.2016.2575241.
[30] M.M. Salour, G. Schoner, M. Kull, J.H. Bechtel, Semiconductor-platelet fibre-optic temperature sensor, Electron. Lett. 21 (1985) 135–136.
[31] K. Kyuma, S. Tai, T. Sawada, M. Nunoshita, Fiber-optic instrument for temperature measurement, IEEE Trans. Microw. Theory Tech. 30 (1982) 522–525, http://dx.doi.org/10.1109/TMTT.1982.1131092.
[32] É. Pinet, S. Ellyson, F. Borne, Temperature fiber-optic point sensors: commercial technologies and industrial applications, Inf. MIDEM. 40 (2010) 273–284.
[33] Y. St-Amant, D. Gariépy, D. Rancourt, Intrinsic properties of the optical coupling between axisymmetric Gaussian beams, Appl. Opt. 43 (2004) 5691–5704, http://dx.doi.org/10.1364/AO.43.005691.

Microrefractometer Based on Off-Center Polymer Caps Bonded Onto Optical Fiber Tips

Oskar Arrizabalaga, Joseba Zubia, and Joel Villatoro

***Abstract*—In this study, we report on a microscopic refractometer built with off-center polymer spherical caps bonded on the end facet of a standard single-mode fiber (SMF). To achieve such microcaps, sub nanoliter amounts of UV-curable polymer were deposited onto the tip of SMFs that were cleaved with small angles. The working mechanism of our devices is explained as the interference of two Gaussian beams. High-contrast (visibility) interference patterns were achieved by optimizing the size of the polymer microcaps. The microrefractometers introduced here can operate over a broad wavelength range from 800 to 1600 nm approximately. The measuring refractive index range of our devices goes from 1 up to the index of the polymer. The refractive index sensitivity is high ($\sim 10^{-4}$) over the whole measuring range. Temperature and refractive index cause two distinct effects on the interference patterns. Thus, our microrefractometers can be temperature self-compensated. Owing to the microscopic size of the refractometers, they can be ideal candidates to monitor refractive index in small spaces such as microfluidic channels. Other microsensors can be developed with suitable polymers or other materials that can be bonded on optical fiber tips.**

***Index Terms*—Interferometry, microsensors, optical fiber sensors, polymer cavities, refractive index sensing, refractometers.**

I. Introduction

REFRACTIVE index (RI) is a unique characteristic of substances, thus, its measurement or monitoring is crucial in a myriad of industrial or scientific applications. For more than a century, the most successful technique to measure the RI of liquids consists of determining the critical angle in an internal reflection configuration [1]–[3]. To do so, sophisticated opto-mechanical or digital instruments are necessary. Such instruments (refractometers), typically use a fixed wavelength, involve a high-RI prism, and a system to heat or cool the sample.

Refractometers based on critical angle measurements can measure RI over a broad range, typically from 1 up to an index close to that of the glass the prism is made of [1], [2]. The resolution that such refractometers achieve is between 10^{-3} to 10^{-5}. Miniaturization of prism-based refractometers to microscopic dimensions without sacrificing resolution and measuring range has been challenging. Therefore, refractometers based on critical angle measurements are not suitable for new or emerging applications. For example, they cannot be used to monitor RI in microfluidic environments [6]–[8] or other small spaces.

Refractometers based on optical fibers have been proposed as an alternative to prism-based ones. Due to the high quality and microscopic dimensions of optical fibers, these types of refractometers are considered good candidates for the new challenges in refractometry. Current fiber-based refractometers (RI sensors) can be classified in three main categories. The first one exploits the interaction of evanescent waves of the guided light with the liquid or sample under study. Such interaction can be achieved with tapered or polished fibers [8]–[13] mode interferometers [14]–[18] or gratings [19]–[24]. The second category is based on Fabry- Perot interferometry (FPI) [25]–[30]. The last category exploits the RI dependence of Fresnel reflection coefficients [31]–[35].

The main disadvantage of refractometers based on evanescent wave interaction is the fact that they provide high resolution (higher than 10^{-4}) only for indices close to the RI of the fiber cladding [8]–[24] which is typically around 1.45. Moreover, the zone of interaction has a length of several millimeters, and even of centimeters. In addition, they are highly sensitive to temperature for which they require a temperature compensation mechanism. On the other hand, refractometers based on FPI measure either shift or visibility changes of an interference pattern as a function of RI [25]–[30]. The drawback of most FPI-based refractometers proposed until now is their limited RI measuring range, their ambiguity, i.e., two distinct indices can give the same value of visibility, or the complex fabrication process to achieve uniform cavities. On the other hand, refractometers based Fresnel reflections tend to require complex interrogation to fully compensate fluctuations of the optical source or to uncontrollable losses in the optical fiber [31]–[35].

In this work, we demonstrate a cost-effective and accurate interferometric fiber optic microrefractometer. It comprises an off-center polymer microcap as the key element. The fabrication of our microrefractometer is simple and reproducible. The

Manuscript received January 31, 2018; revised April 6, 2018 and May 11, 2018; accepted May 26, 2018. Date of publication May 30, 2018; date of current version July 12, 2018. This work was supported in part by the Fondo Europeo de Desarrollo Regional, in part by the Ministerio de Economía y Competitividad under Grant TEC2015-638263-C03-1-R, in part by the Gobierno Vasco/Eusko Jaurlaritza under Grant IT933-16, and in part by the ELKARTEK under Grant KK-2016/0030, Grant KK-2017/00033, Grant KK-2017/00089, and Grant KK-2016/0059. The work of O. Arrizabalaga was supported by the Gobierno Vasco/Eusko Jaurlaritza. *(Corresponding author: Oskar Arrizabalaga.)*

O. Arrizabalaga and J. Zubia are with the Department of Communications Engineering, University of the Basque Country, E-48013 Bilbao, Spain (e-mail: oskar.arrizabalaga@ehu.eus; joseba.zubia@ehu.es).

J. Villatoro is with the Department of Communications Engineering, University of the Basque Country, E-48013 Bilbao, Spain, and also with the IKERBASQUE—Basque Foundation for Science, E-48011 Bilbao, Spain (e-mail: agustinjoel.villatoro@ehu.eus).

Color versions of one or more of the figures in this paper are available online at http://ieeexplore.ieee.org.

Digital Object Identifier 10.1109/JLT.2018.2842121

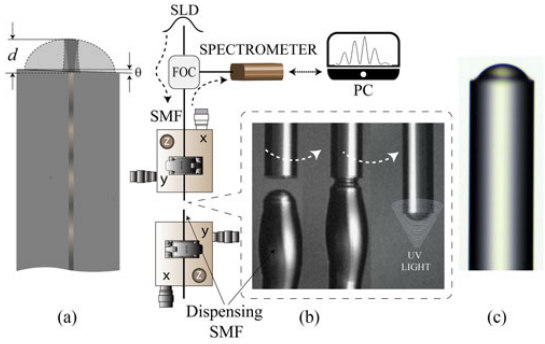

Fig. 1. (a) Illustration of the off-center polymer microcap; d is the height of the microcap and θ is the cleave angle of the SMF. (b) Schematic representation of the set-up used to monitor the fabrication process and to interrogate the samples. The micrographs show the sensor fabrication steps. (c) Micrograph of an SMFwith a 40 μm-long polymer cap. SLD is superluminescent diode, SMF, single mode fiber, FOC, fiber optic coupler, and PC, personal computer.

microcap is achieved by dispensing sub nano-liter amounts of UV-curable polymer onto the end face of a conventional single mode fiber (SMF) which is cleaved at a small angle. The reference beam of the microinterferometer is the light reflected from the SMF-polymer interface and the sensing beam is the light reflected from the polymer-liquid (sample) interface. We found that the small cleave angle along with the size and shape of the polymer microcap were crucial to tailor the contrast or visibility of the interference patterns.

The distinct features of the microrefractometers introduced here include, *i*) microscopic size; *ii*) operation over a wide wavelength range, from 800 to 1600 nm, approximately; *iii*) broad RI measuring range without ambiguity; from 1 up to a RI close to the index of the polymer; *iv*) high sensitivity (10^{-4}) over the whole measuring range; *v*) self-compensation of temperature, thus, eliminating heating or cooling systems or additional reference temperature sensors.

We believe that with suitable polymers that can be bonded on the tip of an optical fiber, the concept and approach reported here can be used to develop a myriad of microsensors for chemical or physical parameters, such as gases, pressure, etc.

II. Device Concept and Fabrication

Our device consists of a polymer microcap bonded on the cleaved end of a single mode fiber (SMF) whose core diameter was 4.4 or 9 μm and the cladding diameter was 125 μm. An illustration of the device is shown in Fig. 1(a). To achieve reproducible devices we implemented the set up depicted in Fig. 1(b). Our set up included two 3-axis optical fiber alignment stages (ULTRAlignTM from Newport), a super luminescent diode (SLD) with peak emission at 850 or 1550 nm as a light source, and suitable optical fiber couplers. In addition, our set up had a compact spectrometer (I-MON 512 USB from Ibsen Photonics, or a CCS175/M from Thorlabs) and a CMOS camera (DCU224C from Thorlabs) connected to a personal computer. In this manner, we could monitor the fabrication process in real time.

The first step of the fabrication process was the cleaving of two SMFs. One of the SMFs was used as a dispensing fiber and the other was the SMF on which we wanted to bond the polymer microcap. To cleave the SMFs we used a cleaver from Fujikura, model CT-32. Such a cleaver provides a typical cleave angle of $\sim$0.5°. The cleaved angles were inspected in a fusion splicer (Fujikura 100P+). For higher reproducibility, we believe that a fiber polishing machine can be used as in such machines the angle of the fiber facet can be selected or fixed.

After the cleaving process, the SMF tips where cleaned with alcohol in an ultrasonic cleaner. The tip of the SMF used as dispenser fiber was dipped into liquid polymer (NOA81, Norland Products Inc.). After withdrawing the SMF from the polymer, a liquid micro-droplet was formed on the SMF tip, but the sides of the SMF were also coated with polymer, see Fig. 1(b). Due to gravity or vibrations, the liquid polymer on the SMF sides can reach, in a matter of seconds, the fiber tip and may increase the size of the droplet. To avoid this, we placed the SMFs in vertical position.

The following step was the deposition of polymer on the SMF that was used as microrefractometer. To do this, the SMF with the polymer droplet and the other SMF were placed face to face and were aligned with the aforementioned 3-axis stages. To place the polymer cap only on the SMF facet, we launched light through FOC to the uncoated SMF and analyzed the interference pattern with the spectrometer, see Fig. 1(b). Due to an air gap between the facet of the uncoated SMF and the polymer droplet, an interference pattern was observed. The alignment was optimal when the interference patterns have high contrast. Next, the SMF with polymer on the tip was moved towards the other SMF until the polymer micro-droplet touched the end face of the uncoated SMF; see Fig. 1(b). The dispensing SMF was then moved away from the other SMF.

Due to surface tension, the polymer dispensed onto the SMF face formed a spherical microcap. From the micrograph shown in Fig. 1(b), it can be noted that the polymer cap is formed only on the end face of the SMF. The final step of the fabrication process consisted in solidifying the polymer microcap. The NOA81 is a polymer that is cured fast with UV light (365 nm). We found that an exposure of the microcap to UV light (CS2010 from Thorlabs) during 30 seconds was sufficient to solidify the polymer. It is important to point out that the bonding between the SMF and the polymer was permanent and strong.

After the UV curing process, the microcaps were inspected with an optical microscope. After a single deposition process, the height of the polymer microcap was $\sim$15 μm. As the diameter of the SMF is 125 μm, thus, the volume of polymer deposited onto the SMF is $\sim$ 0.15 nano-liters. To increase the size and volume of the microcaps we repeated the dispensing process. The deposition of liquid polymer on solid polymer is possible. With our technique, the height of the caps increased at approximately 10 μm each time the dispensing process was repeated. However, the microcaps could not increase to arbitrary dimensions. We observed that SMFs with caps whose height was higher than 45 μm exhibited poor interference patterns, probably due to the strong curvature of the caps. We will see later that for accurate refractometry the fringe contrast of interference patterns is

important. Thus, the fabricated microcaps had a height between 20 and 45 μm.

In the literature, different methods to fabricate polymer optical elements, such as microlenses [36] and single or composite microcavities [37]–[40] onto the facet of a SMF have been reported. The deposition techniques so far reported involve multiple steps such as metal evaporation, manual or dip coating processes, and chemical etching. None of such methods allows the monitoring of the fabrication process in real time. In addition, the face of the SMF must be flat to achieve uniform cavities or lenses with a well-defined shape. A substantial difference of our technique with those previously reported is the fact that we use a SMF cleaved at a small angle that makes the single polymer microcap to be off center. Later, we will discuss the advantages of our approach.

III. Operation Principle

The SMF with a polymer microcap bonded on its cleaved end depicted in Fig. 1(a) can be treated as a two-beam interferometer. As the fiber used is single mode, the two beams that participate in the interference will be considered as Gaussian beams [41]–[43]. The reflection from the SMF-polymer interface is the reference beam of the interferometer. The sensing beam is the fraction of light that is coupled to the SMF core from the reflection from the polymer-external medium interface.

Let us suppose that the Gaussian beam that propagates in the SMF core has a waist radius of ω_0 and an amplitude E_0. Such a beam is partially reflected at the SMF-polymer interface. According to the electromagnetic theory of light, the amplitude of the reflected (reference) beam can be denoted as E_{r1} and can be expressed as:

$$E_{r1} = r_1 E_0. \tag{1}$$

In Eq. (1), r_1 is the amplitude reflection coefficient which depends exclusively on the refractive indices of the polymer (n_p) and the SMF core (n_c) as $r_1 \approx (n_\mathrm{p} - n_\mathrm{c})/(n_\mathrm{p} + n_\mathrm{c})$. The Gaussian beam that leaves from the SMF core broadens due to diffraction. It reaches the polymer-external-medium interface with a waist radius of $\omega_1 = \omega_0[1 + (d\lambda/\pi n_\mathrm{p}\omega_0^2)^2)]^{1/2}$ and an accumulated phase $\phi = 2\pi n_\mathrm{p} d/\lambda$. In these expressions, d is the height of the polymer microcap and λ the wavelength of the optical source. The transmitted Gaussian beam suffers Fresnel reflection from the polymer-external-medium interface. The amplitude of the reflected beam (E_{r2}) can be expressed as $E_{r2} = r_2 E_0(1 - r_1)\exp(-i\phi)$. The amplitude reflection coefficient, r_2, depends exclusively on n_p and the refractive index of the external medium (n_e) as $r_2 \approx (n_\mathrm{p} - n_\mathrm{e})/(n_\mathrm{p} + n_e)$. The waist radius of the reflected Gaussian beam that reaches the SMF core can be denoted as ω_2. The latter can be expressed in a similar manner than ω_1. It is important to point out that the expressions for r_1 and r_2 are valid for quasi-perpendicular incidence.

In an ideal case, all the optical power of the reflected beam from the polymer-external medium interface is coupled in the SMF core. However, due to the broadening of the Gaussian beam along with the angular misalignment of the two reflecting surfaces, only a fraction of optical power can be coupled to the SMF core. The amplitude of the reflected beam that is coupled back to the SMF core can be expressed as:

$$E_c = \eta r_2 E_0 (1 - r_1)^2 \exp(-i2\varphi). \tag{2}$$

In Eq. (2), η is the coupling coefficient. It depends on the cleave angle of the SMF, n_p, d, λ, ω_0, and ω_2, it can be calculated with Eqs. (A7) and (A8) given in Ref. [42]. In Eq. (2), we have assumed that the polymer is transparent in the wavelength range in which we carried out the measurements. Note that E_c can be considered as the sensing beam of the interferometer.

The amplitude of the total reflected field (E_T) is then the sum of the reference (E_{r1}) and the sensing beam (E_c). This means,

$$E_T = E_0 \left[r_1 + \eta r_2 (1 - r_1)^2 \exp(-i2\varphi) \right]. \tag{3}$$

The total reflected intensity that can be measured is then $|E_T|^2$ which, by defining $I_\mathrm{r} = (E_T/E_0)^2$, can be expressed as:

$$I_r = r_1^2 + \eta^2 r_2^2 (1 - r_1)^4 + 2\eta r_1 r_2 (1 - r_1)^2 \cos(2\varphi). \tag{4}$$

The fringe visibility (V) of an interference pattern is defined as the difference over the sum between the maximum and minimum of I_r. Thus, from Eq. (4), V is derived as

$$V = \frac{4\eta(1 - r_1)\sqrt{r_1 r_2}}{2r_1 + 2\eta^2(1 - r_1)^2 r_2}. \tag{5}$$

From Eq. (5), it is clear that the liquid or sample RI (n_e) can be calculated by monitoring the maxima and minima of the reflection spectra. To do so, a low-resolution spectrometer can be used. Note also that the coupling factor plays an important role on V, hence, on the performance of the refractometers.

The RI of the SMF and the polymer depend on the wavelength of the optical source. For a conventional SMF such a dependence is well known. According to the polymer manufacturer, $n_\mathrm{p} = A + B/\lambda^2 + C/\lambda^4$, with $A = 1.5375$, $B = 8290.45$, and $C = -2.11046 \times 10^8$. Thus, at $\lambda = 1550\,\mathrm{nm}$, $n_\mathrm{p} = 1.5409$.

IV. Results and Discussion

In the literature, there are published works that describe interferometers fabricated at the tip of an optical fiber for refractive index sensing [27]–[30], [40]. The main drawbacks of such works is the need of complex fabrication process to achieve composite or micro-structured cavities [27]–[30], the limited range of indices that can be monitored, or the ambiguity of the measurements. For example, two different indices give the same value of visibility [40]. In addition, the effect of temperature is not fully compensated. Therefore, there is need of miniature fiber optic refractometers that rival in performance to those previously reported without the drawbacks mentioned above. Such needs motivated the present work. We placed special emphasis on the design of the microinterferometers and on their fabrication. Next, we discuss our results.

In Fig. 2(a) we show the theoretical value of I_r for different values of n_e when $\eta = 0.18$. In Fig. 2(b) we show V versus RI for different values of η. The dashed- and dotted-line curves shown in Fig. 2(b) could represent the cases of efficient coupling. This means, the case when the external surface of the

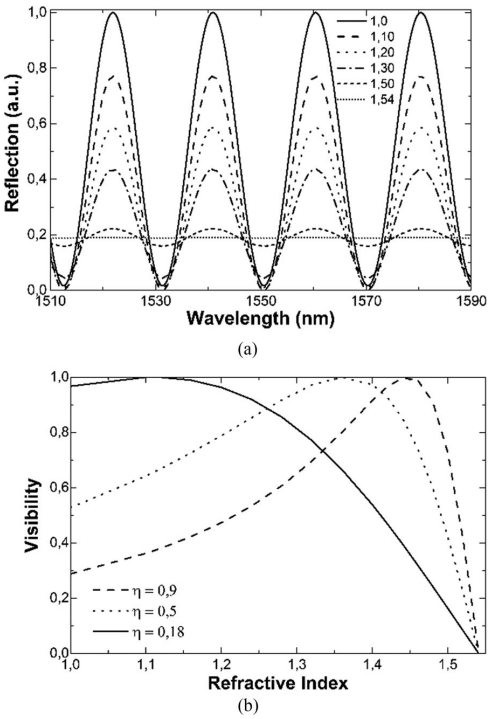

Fig. 2. (a) Spectra at different refractive indices (n_e) calculated from Eq. (4) when $\eta = 0.18$. (b) Theoretical visibility vs refractive index for different values of η.

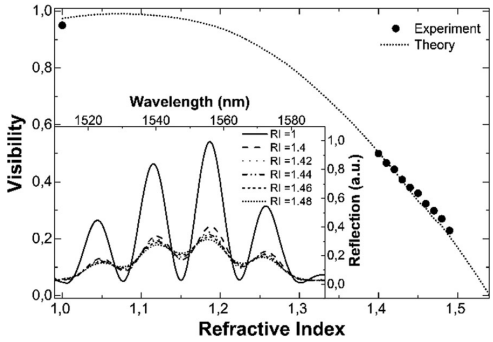

Fig. 3. Visibility as a function of refractive index observed in a sample with a cap of $d = \sim 40\ \mu$m. The dotted line is the theoretical value calculated from Eq. (5) when $\eta = 0.18$. The inset graph shows the observed spectra at different indices.

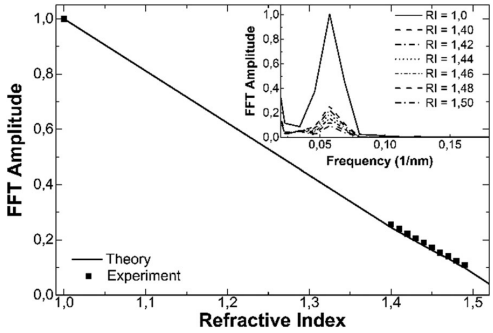

Fig. 4. Amplitude of the fast Fourier transform (FFT) as a function of refractive index. Squares are experimental points and the solid line is the theoretical prediction. The inset shows the FFT as a function frequency for different indices.

polymer microcap is parallel or well aligned to the facet of the SMF. Such a situation can be achieved when the cleave angle (θ) of the SMF is 0° and the caps are small [40], [41]. Note that in this case, the dependence of *V* on n_e is nonlinear. As a result, two different indices given the same value of *V*. This ambiguity make refractometers with centered polymer microcaps impractical [40]. However, when the polymer microcap is off center, see the continuous line of Fig. 2(b), the ambiguity is eliminated or minimized.

Based on the previous analysis, we fabricated several samples in which the cleave angle of the SMF was 0.5° approximately. Such a cleave angle is the typical value that is provided by the cleaver we used. The deposition of polymer on the SMF tip was as described above. To evaluate our microinterferometers as a RI meters, we immersed the polymer-coated SMF tip in calibrated refractive index liquids (from Cargille Labs). Due to limitations, the calibration was done from 1.40 to 1.49 in steps of 0.1. Between consecutive measurements, we cleaned the SMF tip and ensured that the interference pattern returned to its baseline. The measurements were carried out at constant temperature (26.7 °C).

In Fig. 3, we show some spectra observed at different indices. Due to the Gaussian emission of the light source used in the experiments the peaks of interference pattern have not the same amplitude. However, it can be seen how the interference pattern shrinks as the RI increases. The calibration curve, i.e., visibility as a function of RI, is shown in the figure. The dotted line shown in the figure is the theoretical value calculated from Eq. (5) with $\eta = 0.18$ which is turn was calculated from Eqs. A7 and A8 provided in Ref. [42]. It can be noted the good agreement between experiment and theory.

As the dependence of *V* on n_e is nonlinear in the region around 1.1, we explored other possibilities to extract information of RI from the interference patterns. We found that by means of the fast Fourier transform (FFT) the nonlinear response can be eliminated. In Fig. 4 we show the amplitude of the FFT as a function of n_e. The FFT was taken from the spectra shown in the inset of Fig. 3. In the Fourier domain, a single peak was observed. The amplitude of the FFT is the height of such a peak; it is not affected by the shift of the interference pattern. Again, the calibration curve agrees well with the theoretical value of the FFT amplitude. Note the linear response of the FFT amplitude (F_n) as a function of n_e.

By normalizing, i.e., by considering that $F_n = 1$ when $n_e = 1$, F_n as a function of n_e can be expressed as

$$F_n = 1 - S_n\,(n_e - 1)\,. \tag{6}$$

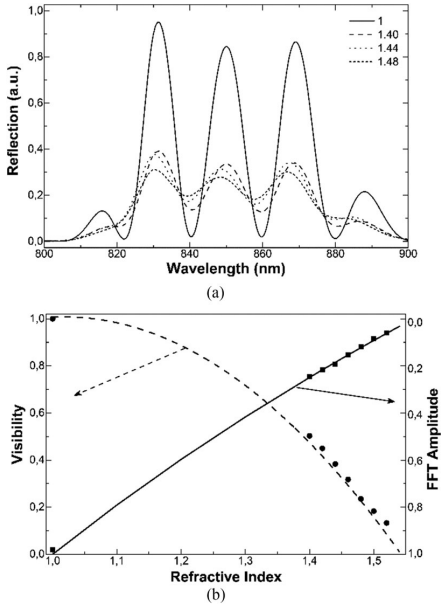

Fig. 5. (a) Spectra observed at different refractive index. The cavity length was $\sim$20 μm. (b) Visibility (dots) and FFT amplitude (squares) as a function of refractive index. The solid and dashed lines are the calculated curves by assuming $d = 20$ μm and $\eta = 0.18$.

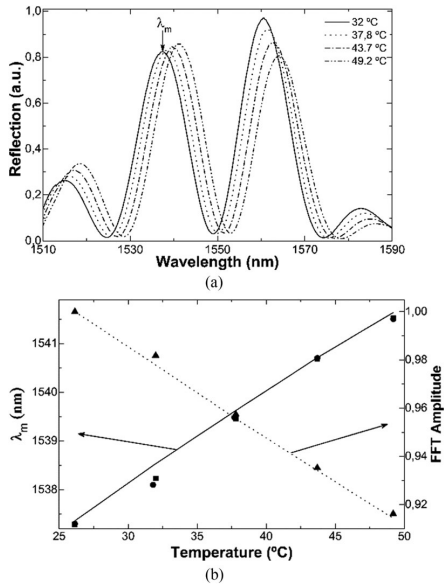

Fig. 6. (a) Reflection spectra observed at different temperatures. λ_m is the position of a maximun of the interference pattern. (b) Position of λ_m and FFT amplitude as a function of temperature. Squares (heating) and dots (cooling) are triangles (heating) are experimental values. The solid and dashed lines are theoretical predictions. The cavity size was 40 μm.

This means that the calibration of our microrefractometer requires knowledge of only one value (the refractive index of air). We believe that such calibration is straightforward. Note from Fig. 4, we can see that $S_n = 1/(n_p - 1)$. Thus, when $n_e = n_p$, $F_n = 0$. S_n is the RI sensitivity. This means that the sensitivity of our microrefractometer and the measuring range can be tuned with the polymer RI. Thus, a refractometer with microcap made of low-index polymer will have higher sensitivity and narrower measuring range than one with a cap made of high-index polymer. The FFT amplitude can be determined with high precision; thus, the estimated resolution of our refractometer is 10^{-4} over the whole measuring range. Such a resolution is high enough for most industrial applications.

We also fabricated some samples with single mode fiber at 850 nm (780 HP from Thorlabs). The cleaving of such an SMF was also made with the cleaver aforementioned. The cleave angle was again 0.5°. The deposition of the polymer on the fiber facet was carried out with the process described above. The advantage in this case is the low cost of the mid-resolution spectrometer necessary to interrogate the devices. As the wavelength is shorter the period of the interference pattern is shorter.

Figure 5(a) shows the spectra of a sample with a cap of $d \sim 20$ μm for different values of n_e. Note that maximum visibility is achieved when $n_e = 1$. The visibility and FFT amplitude as a function of n_e are shown in Fig. 5(b). Again, our theoretical results agree well with the experimental ones. The dependence of the FFT amplitude on n_e can also be described with Eq. (6), the only difference is the value of the n_p at $\lambda = 850$ nm.

The temperature effect on our devices was also studied. Temperature (T) modifies the RI of the polymer and the size of the cavity as follows:

$$n_p(T) = n_0(T_0) + (\partial n_p/\partial T)_{T=T_0}(T - T_0) \tag{7}$$

$$d(T) = d_0(T_0)\,[1 + \alpha_T(T - T_0)] \tag{8}$$

In Eq. (7) and (8), $(\partial n_p)/\partial T$ is the thermo-optic coefficient (TOC) and αT is the thermal expansion coefficient (TEC). For the NOA81, the TOC $= -1.83 \times 10^{-4}$ and the TEC $= 2.4 \times 10^{-4}$.

Figure 6(a) shows the interference patterns of a sample with $d = 40$ μm at different temperatures. The position of a local maximum of the interference pattern is denoted as λ_m. It can be observed that as the temperature increases the interference pattern shifts to longer wavelengths. Fig. 6(b) shows the position of λ_m as a function of temperature. The calibration curve gave us a temperature sensitivity of 197 pm/°C. In the figure, we also show the FFT amplitude (F_T) as a function of temperature.

From the figure, we get the following relationship between F_T and temperature (T):

$$F_T = 1 - S_{FT}(T - T_0) \tag{9}$$

In Eq. (9), S_{FT} is the thermal sensitivity and we have assumed that the FFT amplitude at temperature $T_0 = 25$ °C is 1.

From the calibration curve shown in Fig. 6, $S_{FT} = (1 - F_{Tx})/(T_x - T_0)$, with Tx an arbitrary temperature and F_{Tx} the value of the FFT amplitude at Tx. In our case S_{FT} was found to be -0.004/°C. Although the FFT amplitude changes little

with temperature, it can cause errors in the measurements of RI. Thus, the amplitude of the FFT when n_e and T change can be expressed as:

$$F_{nT}(n_e, T) = 1 - [S_n(n_e - 1) - S_{FT}(T - T_0)]. \quad (10)$$

It is interesting to note that n_e does not shift the interference pattern, but temperature does. Therefore, by monitoring the shift of the interference pattern, or the position of λ_m, T can be known, hence F_{nT} and the external refractive index at any temperature. Therefore, the microrefractometer here proposed can be self-temperature compensated.

V. Conclusions

We have reported on an accurate interferometric fiber optic refractive index sensor which has micrometer size. Our sensor provides linear response, broad refractive index measuring range, and high sensitivity over the whole measuring range. The fabrication of the sensors is simple and reproducible. An important advantage is that they operate at the well-established telecommunications wavelengths. In our microrefractometers, the key element is an off-center polymer microcap bonded onto the facet of a single mode optical fiber.

We believe that the devices here proposed can be useful in several applications that demand ultra miniature refractive index meters. For example, they can useful to monitor index of liquids inside micro-fluid channels or in other small spaces.

Their passive nature makes them attractive also in industrial applications. Presently, polymers with tailored optical and physical properties can synthetized. Therefore, the performance of the sensors here proposed can be further improved.

Other applications that we foresee are in the field of biochemical sensing. In these applications, polymers permeable to chemical or biological parameters will be required. Under the presence of such parameters, the polymer refractive index can change. Such changes can be detected or monitored with the techniques reported here.

References

[1] J. Rheims, J. Köser, and T. Wriedt, "Refractive-index measurements in the near-IR using an Abbe refractometer," *Meas. Sci. Technol.*, vol. 8, no. 6, pp. 601–605, 1997.

[2] M. H. Chiu, J. Y. Lee, and D. C. Su, "Refractive-index measurement based on the effects of total internal reflection and the uses of heterodyne interferometry," *Appl. Opt.*, vol. 36, no. 13, pp. 2936–2939, 1997.

[3] S. Kedenburg, M. Vieweg, T. Gissibl, and H. Giessen, "Linear refractive index and absorption measurements of nonlinear optical liquids in the visible and near-infrared spectral region," *Opt. Mater. Exp.*, vol. 2, no. 11, pp. 1588–1611, 2012.

[4] L. Lei, H. Li, J. Shi, and Y. Chen, "Microfluidic refractometer with integrated optical fibers and end-facet transmission gratings," *Rev. Sci. Instrum.*, vol. 81, no. 2, 2010, Art. no. 023103. [Online]. Available: https://doi.org/10.1063/1.3280226

[5] S. Y. Yoon and S. Yang, "Microfluidic refractometer with micro-image defocusing," *Lab Chip*, vol. 11, no. 5, pp. 851–855, 2011.

[6] P. Polynkin, A. Polynkin, N. Peyghambarian, and M. Mansuripur, "Evanescent field-based optical fiber sensing device for measuring the refractive index of liquids in microfluidic channels," *Opt. Lett.*, vol. 30, no. 11, pp. 1273–1275, 2005.

[7] A. Kumar, T. V. B. Subrahmanyam, A. D. Sharma, K. Thyagarajan, B. P. Pal, and I. C. Goyal, "Novel refractometer using a tapered optical fibre," *Electron. Lett.*, vol. 20, no. 13, pp. 534–535, 1984.

[8] D. Monzón-Hernández, J. Villatoro, and D. Luna-Moreno, "Miniature optical fiber refractometer using cladded multimode tapered fiber tips," *Sens. Actuators B, Chem.*, vol. 110, no. 1, pp. 36–40, 2005.

[9] J. Wo *et al.*, "Refractive index sensor using microfiber-based Mach–Zehnder interferometer," *Opt. Lett.*, vol. 37, no. 1, pp. 67–69, 2012.

[10] K. Schroeder, W. Ecke, R. Mueller, R. Willsch, and A. Andreev, "A fibre Bragg grating refractometer," *Meas. Sci. Technol.*, vol. 12, no. 7, pp. 757–764, 2001.

[11] G. Quero *et al.*, "Evanescent wave long-period fiber grating within D-shaped optical fibers for high sensitivity refractive index detection," *Sens. Actuators B, Chem.*, vol. 152, no. 2, pp. 196–205, 2011.

[12] Y. Jung, S. Kim, D. Lee, and K. Oh, "Compact three segmented multimode fibre modal interferometer for high sensitivity refractive-index measurement," *Meas. Sci. Technol.*, vol. 17, no. 5, pp. 1129–1133, 2006.

[13] R. Jha, J. Villatoro, G. Badenes, and V. Pruneri, "Refractometry based on a photonic crystal fiber interferometer," *Opt. Lett.*, vol. 34, no. 5, pp. 617–619, 2009.

[14] Q. Wu, Y. Semenova, P. Wang, and G. Farrell, "High sensitivity SMS fiber structure based refractometer—Analysis and experiment," *Opt. Exp.*, vol. 19, no. 9, pp. 7937–7944, 2011.

[15] G. Salceda-Delgado, D. Monzon-Hernandez, A. Martinez-Rios, G. A. Cardenas-Sevilla, and J. Villatoro, "Optical microfiber mode interferometer for temperature-independent refractometric sensing," *Opt. Lett.*, vol. 37, no. 11, pp. 1974–1976, 2012.

[16] A. Datta and A. Saha, "Investigation of a multimode interference-based high-sensitivity refractive index sensor realized by shining a zero-order Bessel–Gauss beam," *J. Opt. Soc. Amer. B*, vol. 34, no. 7, pp. 1327–1339, 2017

[17] V. Bhatia and A. M. Vengsarkar, "Optical fiber long-period grating sensors," *Opt. Lett.*, vol. 21, no. 9, pp. 692–694, 1996.

[18] T. Allsop, R. Reeves, D. J. Webb, I. Bennion, and R. Neal, "A high sensitivity refractometer based upon a long period grating Mach-Zehnder interferometer," *Rev. Sci. Instrum.*, vol. 73, no. 4, pp. 1702–1705, 2002.

[19] F. Shen, C. Wang, Z. Sun, K. Zhou, L. Zhang, and X. Shu, "Small-period long-period fiber grating with improved refractive index sensitivity and dual-parameter sensing ability," *Opt. Lett.*, vol. 42, no. 2, pp. 199–202, 2017.

[20] X. Fang, C. R. Liao, and D. N. Wang, "Femtosecond laser fabricated fiber Bragg grating in microfiber for refractive index sensing," *Opt. Lett.*, vol. 35, no. 7, pp. 1007–1009, 2010.

[21] W. Zhou, Y. Zhou, and J. Albert, "A true fiber optic refractometer," *Laser Photon. Rev.*, vol. 11, no. 1, p. 1600157, 2017.

[22] B. Jiang, K. Zhou, C. Wang, Y. Zhao, J. Zhao, and L. Zhang, "Temperature-calibrated high-precision refractometer using a tilted fiber Bragg grating," *Opt. Exp.*, vol. 25, no. 21, pp. 25910–25918, 2017.

[23] S. D. Woodruff and E. S. Yeung, "Refractive index and absorption detector for liquid chromatography based on Fabry–Perot interferometry," *Anal. Chem.*, vol. 54, no. 7, pp. 1174–1178, 1982.

[24] R. Gao, Y. Jiang, W. Ding, Z. Wang, and D. Liu, "Filmed extrinsic Fabry–Perot interferometric sensors for the measurement of arbitrary refractive index of liquid," *Sens. Actuators, B Chem.*, vol. 177, pp. 924–928, 2013.

[25] Z. L. Ran, Y. J. Rao, W. J. Liu, X. Liao, and K. S. Chiang, "Laser-micromachined Fabry–Perot optical fiber tip sensor for high-resolution temperature-independent measurement of refractive index," *Opt. Exp.*, vol. 16, no. 3, pp. 2252–2263, 2008.

[26] S. Pevec and D. Donlagic, "High resolution, all-fiber, micro-machined sensor for simultaneous measurement of refractive index and temperature," *Opt. Exp.*, vol. 22, no. 13, pp. 16241–16253, 2014.

[27] J. Tian, Y. Lu, Q. Zhang, and M. Han, "Microfluidic refractive index sensor based on an all-silica in-line Fabry–Perot interferometer fabricated with microstructured fibers," *Opt. Exp.*, vol. 21, no. 5, pp. 6633–6639, 2013.

[28] P. Chen, X. Shu, H. Cao, and K. Sugden, "High-sensitivity and large-dynamic-range refractive index sensors employing weak composite Fabry–Perot cavities," *Opt. Lett.*, vol. 42, no. 16, pp. 3145–3148, 2017.

[29] J. R. Zhao, X. G. Huang, and J. H. Chen, "A Fresnel-reflection-based fiber sensor for simultaneous measurement of liquid concentration and temperature," *J. Appl. Phys.*, vol. 106, no. 8, p. 083103, 2009.

[30] J. R. Zhao, X. G. Huang, W. X. He, and J. H. Chen, "High-resolution and temperature-insensitive fiber optic refractive index sensor based on Fresnel reflection modulated by Fabry-Perot interference," *J. Lightw. Technol.*, vol. 28, no. 19, pp. 2799–2803, Oct. 2010.

[31] W. Xu, X. G. Huang, and J. S. Pan, "Simple fiber-optic refractive index sensor based on Fresnel reflection and optical switch," *IEEE Sensors J.*, vol. 13, no. 5, pp. 1571–1574, May 2013.
[32] M. G. Shlyagin, R. Martínez Manuel, and O. Esteban, "Optical-fiber self-referred refractometer based on Fresnel reflection at the fiber tip," *Sens. Actuators B, Chem.*, vol. 178, pp. 263–269, 2013.
[33] A. Basgumus, F. E. Durak, A. Altuncu, and G. Yilmaz, "A universal and stable all-fiber refractive index sensor system," *IEEE Photon. Technol. Lett.*, vol. 28, no. 2, pp. 171–174, Jan. 2016.
[34] K. R. Kim, S. Chang, and K. Oh, "Refractive microlens on fiber using UV-curable fluorinated acrylate polymer by surface-tension," *IEEE Photon. Technol. Lett.*, vol. 15, no. 8, pp. 1100–1102, Aug. 2003.
[35] P. C. Beard and T. N. Mills, "Miniature optical fibre ultrasonic hydrophone using a Fabry-Perot polymer film interferometer," *Electron. Lett.*, vol. 33, no. 9, pp. 801–803, 1997.
[36] F. J. Arregui, I. R. Matías, and R. O. Claus, "Optical fiber gas sensors based on hydrophobic alumina thin films formed by the electrostatic self-assembly monolayer process," *IEEE Sensors J.*, vol. 3, no. 1, pp. 56–61, Feb. 2003.
[37] J. Liu, Y. Sun, and X. Fan, "Highly versatile fiber-based optical Fabry–Pérot gas sensor," *Opt. Exp.*, vol. 17, no. 4, pp. 2731–2738, 2009.
[38] X. L. Tan, Y. F. Geng, X. J. Li, Y. L. Deng, Z. Yin, and R. Gao, "UV-curable polymer microhemisphere-based fiber-optic Fabry–Perot interferometer for simultaneous measurement of refractive index and temperature," *IEEE Photon. J.*, vol. 6, no. 4, Aug. 2014, Art. no. 7800208.
[39] B. Sun *et al.*, "Simultaneous measurement of pressure and temperature by employing Fabry–Perot interferometer based on pendant polymer droplet," *Opt. Exp.*, vol. 23, no. 3, pp. 1906–1911, 2015.
[40] W. P. Chen, D. N. Wang, B. Xu, C. L. Zhao, and H. F. Chen, "Multimode fiber tip Fabry–Perot cavity for highly sensitive pressure measurement," *Sci. Rep.*, vol. 7, no. 1, 2017, Art. no. 368.
[41] S. Nemoto and T. Makimoto, "Analysis of splice loss in single-mode fibres using a Gaussian field approximation," *Opt. Quantum Electron.*, vol. 11, no. 5, pp. 447–457, 1979.
[42] Y. St-Amant, D. Gariépy, and D. Rancourt, "Intrinsic properties of the optical coupling between axisymmetric Gaussian beams," *Appl. Opt.*, vol. 43, no. 30, pp. 5691–5704, 2004.
[43] P. R. Wilkinson and J. R. Pratt, "Analytical model for low finesse, external cavity, fiber Fabry–Perot interferometers including multiple reflections and angular misalignment," *Appl. Opt.*, vol. 50, no. 23, pp. 4671–4680, 2011.

Authors' biographies not available at the time of publication.

Sensors & Actuators: B. Chemical 297 (2019) 126700

Contents lists available at ScienceDirect

Sensors and Actuators B: Chemical

journal homepage: www.elsevier.com/locate/snb

Miniature interferometric humidity sensor based on an off-center polymer cap onto optical fiber facet

Oskar Arrizabalaga[a,*], Javier Velasco[b], Joseba Zubia[a], Idurre Sáez de Ocáriz[b], Joel Villatoro[a,c]

[a] Department of Communications Engineering, Escuela de Ingenieria de Bilbao, University of the Basque Country UPV/EHU, Plaza Ingeniero Torres Quevedo 1, E-48013 Bilbao, Spain
[b] Fundación Centro de Tecnologías Aeronáuticas (CTA), Miñano, Spain
[c] IKERBASQUE -Basque Foundation for Science, E-48011 Bilbao, Spain

ARTICLE INFO

Keywords:
Optical fiber sensors
Interferometers
Microsensors
Polymer cap
Humidity sensors

ABSTRACT

In this work, we propose an interferometric humidity sensor based on a polymer micro-cap bonded off-center on the polished end of a standard single mode fiber (SMF). In our sensor, the sensitive part is the micro-cap. In the interferometer fabrication process, we can adjust the misalignment between the core and the micro-cap. It allowed us to control the visibility of the interference pattern. In our device, water molecules absorbed by the polymer microcap causes changes in the height of the microcap. This results in measurable shifts of the interference pattern. The fabricated samples were tested in a calibrated climatic chamber in the range from ˜10 to ˜95% of relative humidity (RH). The sensitivity and resolution of our device was found to be 148 pm per %RH and 0.04% RH, respectively. The obtained results suggest that our sensors can be useful to monitor relative humidity (RH) in miniature spaces.

1. Introduction

Humidity measurements have relevant importance in many areas of applications including, for example, manufacturing processes, [1] breath monitoring [2–5], or meteorological studies [6]. Every of such application demands specific humidity sensors. Therefore, factors such as range of detection, stability, response and recovery times, sensitivity or accuracy must be tailored when designing a humidity sensor. In addition, cost, simple design, and small size of the sensor are also important.

The most mature technology to develop humidity sensors exploit changes in resistance or capacitance of a humidity-sensitive thin film. The material the film is made of, can be polymer, bio-material, metal oxide, ceramic, or 2D material [7–11]. The physical changes of the thin film induced by humidity are measured by means of electronic technology. Nevertheless, electronic humidity sensors have some drawbacks. For example, they cannot measure humidity levels less than 5%, have nonlinear behavior or hysteresis, and need regular calibration. Besides, electronic humidity sensors may not work or cannot be used in environments where electromagnetic fields are present.

As an alternative to well-established electronic humidity sensors, those based on fiber optics technology have been proposed. Fiber optic humidity sensors have important features such as electromagnetic compatibility, remote sensing and multiplexing capabilities. Additionally, fiber optic humidity sensors have miniature size and are lightweight. As optical fibers are insensitive to humidity, an intermediate hygroscopic material is usually necessary. Such material can be deposited on a section or on the tip of an optical fiber. In this manner, the guided light interacts with the hygroscopic material, which in turn is exposed to humidity. The changes induced by humidity to such material result in measurable changes of the guided light.

Optical absorption is a technique to detect humidity [12–15]. In this technique, the evanescent field of the guided light interacts with the hygroscopic material and the transmitted spectrum is monitored as a function of humidity. The main disadvantage of this technique is that power fluctuations of the light source or curvature in the optical fiber can be misinterpreted as humidity.

Long period gratings (LPGs) [16] coated with a humidity-sensitive material can also be used to detect humidity. In an LPG cladding modes are excited [17], such modes are highly sensitive to changes of refractive index of the material that coats the LPG [18]. Nevertheless, it is difficult to have full control of the cladding modes that are excited with an LPG, thus sensors based on LPGs have low yield [19–22].

Fiber Bragg gratings (FBG) [23] are also widely used to design and fabricate humidity sensors. The working principle of these sensors is based on changes in the Bragg wavelength of the FBG caused by the

* Corresponding author.
E-mail address: oskar.arrizabalaga@ehu.es (O. Arrizabalaga).

https://doi.org/10.1016/j.snb.2019.126700
Received 28 February 2019; Received in revised form 12 June 2019; Accepted 14 June 2019
Available online 17 June 2019

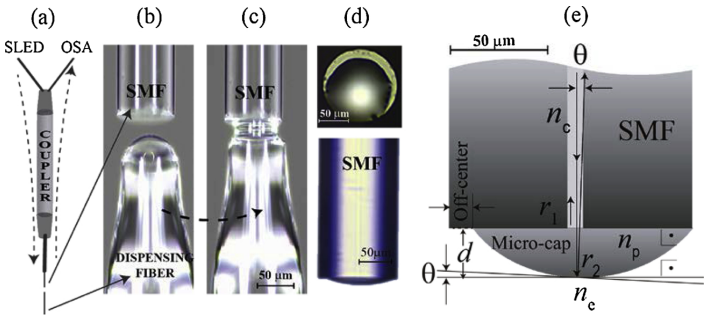

Fig. 1. (a) Schematic representation of the set-up used to monitor the fabrication process and to interrogate devices. (b) and (c) Micrograph of the fabrication steps where the polymer is added to the end face of the SMF.(d) Micrographs of a fabricated sensor sample. On top, frontal view of the off-center of the micro-cap. Below, lateral view of the sensor. (e) Illustration of the theoretical principle of our interferometer.

swelling of a hygroscopic material deposited around the segment of fiber that has the grating [24,25]. An important advantage of FBG sensors is their multiplexing capability. However, FBG humidity sensors have low sensitivity, narrow measuring range, and slow response time [26]. Since different materials possess different swelling properties, many materials have been proposed by different groups in an effort to improve the performance of such humidity sensors [27–29]. Also, different coating methods and thicknesses have also been studied with the aim to improve the sensitivity of FBG humidity sensors [30–32].

Interferometry is another technique widely used for humidity sensing. There are different ways to implement interferometers, as for example, with tapered optical fibers [33,34], photonic crystal fibers [35–37], or with a combination of different types of fibers [38,39]. The main characteristic of most interferometric humidity sensors is their cross sensitivity to humidity and to other parameters such as temperature. An advantage of interferometers is the fact that they can detect humidity even without a hygroscopic material [40]. Interferometric humidity sensors have also some disadvantages. These include low sensitivity to humidity and the narrow humidity range that they can measure [41–43].

Fabry-Perot (FP) cavities are also good alternatives to monitor humidity. In this case, a thin layer of hygroscopic material is deposited on the end face of an optical fiber [44–47]. The advantage of this type of humidity sensors is their miniature size. However, in most cases, the deposition of the material is carried out manually [43,48–51]. Thus, the reproducibility is low [48]. Many research groups have proposed different configuration of FP-based humidity sensors have to improve their performance [52,53], but the thermo-optic (TO) and thermo-expansion (TE) effects on the polymer have not been analyzed. On the other hand, FP-based humidity sensors that can compensate temperature effect, require an additional temperature sensor [49]. Therefore, despite the many advantages that humidity sensors based on optical fibers have, their characteristics must be improved to compete with their electronic sensors counterpart. These characteristic include simpler design and reproducible fabrication methods which may lead to lower sensor costs. Other important factor include high sensitivity and accuracy, wide measurement range, miniature size, no hysteresis, linear behavior, stability, etc.

Based on the aforementioned, in this work, we propose a miniature interferometric humidity sensor. The design of our device is simple which allowed us to achieve high reproducibility. As a hygroscopic material, we used nanoliter amounts of a UV-curable polymer (NOA 81 from Norland Products, Inc) that is commercially available. A simple setup was implemented to monitor the fabrication process in real time. In this manner, we achieved devices with well-defined interference patterns that were analyzed with a low cost spectrometer. In addition, in our devices, the effect of temperature on the polymer micro-cap can be compensated with another interferometer isolated from humidity [54].

According to the manufacturer, the polymer, once cured and aged, can withstand temperatures from −150 °C to 125 °C. Therefore, the devices here proposed are suitable for a myriad of environments or aplications. The fabricated samples were exposed to humidity from 10 to 95% at different temperatures. The obtained results show that our devices are highly sensitive to humidity (148 pm per %RH), are accurate and as fast as a commercial capacitive humidity sensor. In addition, the behavior of our sensor is linear over a broad range of humidity and has no hysteresis. An additional advantage of our humidity sensors is their microscopic dimensions.

2. Sensor fabrication process

The device fabrication consists of the following steps. Firstly, a standard single mode fiber (SMF) was cleaved using a fiber optic cleaver (model CT-32 from Fujikura). After that, the cleaved fiber was polished flat with a fiber optic polishing machine, model NOVA from Krell Tech. Once this was done, the SMF was cleaned and then clamped to an optical fiber alignment stage (ULTRAlign™ from Newport). Additionally, a short piece of cleaved SMF was submerged in a commercial polymer (NOA 81, from Norland Products). The polished and the cleaved SMFs were clamped is separated fiber alignment stages that were in vertical position. The SMF coated with polymer was placed beneath of the polished SMF. Next, light from a super luminescent diode (SLD) source, with peak emission at 850 nm, was launched to the polished SMF end by means of a suitable optical coupler. The interference pattern generated by the two SMF faces was analyzed using a mini spectrometer. Then, the SMF coated with polymer was approached to polished SMF tip until the spectrum from the air gap formed between the end face of the SMF and the polymer had a well-defined interference pattern, see Fig. 1(b).

After this, the fibers were misaligned. The next step was to gently move the dispensing fiber in the direction of the polished SMF until both fibers were in contact, see Fig. 1(c). Then, the dispensing SMF was moved downwards. As a result, an off-center micro-size polymer cap on the end face of the polished SMF was formed, see Fig. 1(d). Finally, to solidify the polymer cap, it was exposed to UV light during a few seconds. By the polymer manufacturer recommendation, for an optimum adhesion, the device was aged at 50 °C during 12 h. In Fig. 1(d), we show micrographs of the front and lateral views of the resulting polymer cap onto the polished SMF.

We would like to point out that the process described above can be carried out automatically. For example, similar opto-mechanical components (mini cameras, translation stages, etc.), techniques, and alignment process implemented in commercial fiber fusion splicers can be adopted to align the dispensing and receiving fibers. Therefore, the fabrication of the devices proposed here can be carried out in seconds.

3. Operation principle

The operating principle of our device is explained as follows. The

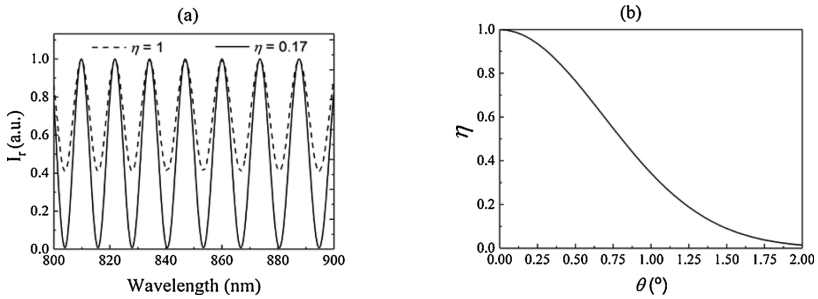

Fig. 2. (a) Theoretical simulation of our interferometric device, calculated from Eq.(5) with an angular misalignment of 1.26° and without angular misalignment, solid and dashed line, respectively. (b) Coupling coefficient versus axial misalignment.

fundamental SMF mode is considered as a Gaussian beam with amplitude E_0. Part of this beam, due to Fresnel reflection, will be reflected towards the SMF core once it reaches the SMF-polymer interface. The amplitude of the reflection is denoted as r_1, see Fig. 2(a). Therefore, the reflected wave, denoted as E_{r1}, can be expressed as:

$$E_{r1} = r_1 E_0, \tag{1}$$

where r_1 is the reflection coefficient and is calculated as $r_1 \approx (n_p - n_c)/(n_p + n_c)$. In the latter equation, n_p and n_c are the refractive index of the polymer and the core of the SMF, respectively. The non-reflected part of the wave will travel in the polymer until it reaches the polymer-SMF interface. As the beam is Gaussian, the waist radius of such a beam can be calculated as $w_1 = w_0[1 + (d\lambda/\pi n_p w_0^2)^2)]1/2$. The accumulated phase of the beam is given by the expression: $\phi = 2\pi n_p d/\lambda$. In the expressions of w_1 and φ, d is the height of the polymer microcap and λ the centered wavelength of the optical source, and is w_0 is the waist of the beam before leaving the SMF core.

After reaching the polymer-external medium interface, the wave will be reflected back due to the Fresnel reflection. The amplitude of the reflected beam can be mathematically written as:

$$E_{r2} = E_0 r_2 (1 - r_1) exp(-i\phi), \tag{2}$$

where r_2 is the reflection coefficient in the interface polymer-outside medium and is calculated as $r_2 \approx (n_e / n_p)/(n_e + n_p)$, being n_e the refractive index of the external medium. The waist radius of E_{r2} beam that reaches the SMF core can be denoted as ω_d. It can be expressed in a similar manner than w_1.

Due to the misalignment of the polymer-cap, the portion of the reflected wave that is coupled in the SMF core will be [55,56]:

$$E_c = \eta r_2 E_0 (1 - r_1)^2 \exp(-i2\phi), \tag{3}$$

where η is the coupling coefficient that can be calculated from Eqs. A7 and A(8) given in reference [55]. It depends strongly on the angular misalignment, θ, see Fig. 1(e). Thus, the amplitude of the total reflected wave (E_T) is the sum of E_{r1} and E_c, that it is:

$$E_T = E_0[r_1 + \eta r_2 (1 - r_1)^2 exp(-i\phi)]. \tag{4}$$

Therefore, the total reflected intensity that can be measured with a light detector can be expressed as $I_r = (E_T/E_0)^2$. The result of this operation turns out to be:

$$I_r = r_1^2 + \eta^2 r_2^2 (1 - r_1)^4 + 2\eta r_1 r_2 (1 - r_1)^2 \cos(2\phi). \tag{5}$$

It can be noted that Eq. (5) is not the typical expression assumed by most authors for Fabry-Perot interferometers [48,57] which is considered as a two beam interferometer. The divergence of the beam that leaves the SMF and the features of the interface of the polymer (or any other material) and the external medium determine the performance of the interferometer, hence of the sensor.

From Eq. (5) it is possible to deduce that the maximums of the I_r will be given when $\varphi = 2m\pi$ and the minimum when $\varphi = (2m + 1)\pi$, m being a positive integer. So, the wavelengths of the interference pattern where I_r takes maximum values will be located at:

$$\lambda_m = (2n_p d)/m \tag{6}$$

The visibility (V) of an interference pattern is defined as the difference over the sum between the maximum and minimum of such a pattern. Thus, from Eq. (5), we can derived V as:

$$V = \frac{4\eta(1 - r_1)\sqrt{r_1 r_2)}}{2r_1 + 2\eta^2(1 - r_1)^2 r_2}. \tag{7}$$

From Eq. (7), it can be deduced that it is possible to achieve a maximum value of V by adjusting the coupling coefficient η, which depends on the axial misalignment θ, n_p, d, λ, ω_0, and w_d [55,58].

According to Eq. (5), the maximum value of V is found when the $\eta = 0.17$. This value was found by calculating η when $\theta = 1.26°$. We also have plotted Eq. (5) when $\theta = 0$, that is when $\eta = 1$. In Fig. 2(a), we have graphed the comparative of both mentioned situations. It can be seen that the visibility increases 40% due to the off-centering of the microcap. Fig. 2(b) shows the strong influence of the misalignment on the coupling coefficient η, and consequently, on the visibility of the interference pattern, see Eq. (7).

4. Experimental results

The polymer that we used to fabricate the micro caps onto the SMF can absorb water molecules [59]. Such polymer swells when it is exposed to relative humidity (RH). Consequently, the height of the microcap d, will increase if RH increases. Thus, our device can be used as a humidity sensor. According to Eq. (6) and, by assuming constant temperature, λ_m will shift to the red if d increases (RH increases), or will shift to the blue if the RH decreases.

Our devices were assessed as humidity sensors in the Aerospace Test Laboratory located in Miñano, Spain. To do so, the interrogation system shown in Fig. 1(a) was used. A broadband light from a super luminescent diode source (SLD), model OFLS- S from Safibra, was launched into the core of the SMF through a suitable optical coupler. By means of a mini-spectrometer (CCS 100 from Thorlabs), one of the maximum wavelengths (λ_m) of I_r, was tracked and analyzed. After that, our devices were placed inside of a calibrated climatic chamber (mode Climacell,- from MMM Group). A capacitive humidity sensor was used as a reference. The climatic chamber was programmed in order to subject our devices to different tests.

In Fig. 3(a), it can be seen the shift of the spectrum of one of our device when it was exposed to different concentration of RH at 22 °C. Note the good agreement between the experimental spectrum and the theoretically calculated spectrum shown in Fig. 2(a). Fig. 3(b) shows the response of our device when it was exposed to RH from ˜10 to ˜95% in steps of 15% and down to ˜10% in the same steps. It can be noted that our device provided information about RH as accurate as the electronic

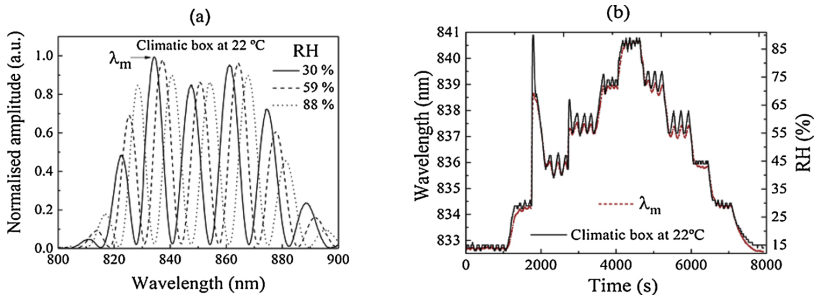

Fig. 3. (a) Spectra at different RH of our sensor, λ_m denotes the tracked maximum. (b) Comparative in real time between our device and the capactive humidity sensor of the calibrated climatic box.

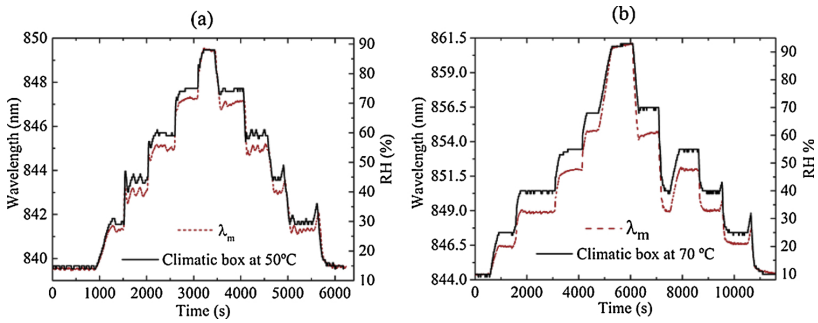

Fig. 4. (a) Comparative in real time between our device and the capactive humidity sensor of the calibrated climatic box at 50 °C. (b) The same comparative that the previous one but with the climatic box at 50 °C.

sensor located in the climatic chamber.

The aforementioned tests, were also carried out at 50 and 70 °C and the results obtained are shown in Figs. 4(a) and 4(b). These graphs show how the tracked wavelength (λ_m) of the spectrum, shifts to the red or to the blue according to the climatic chamber RH variations. From the data of the aforementioned graphs, our sensor was calibrated for each temperature test carried out. The result as summarized in Fig. 5(a). From the sensor calibration, it can be seen that our sensor behaves linearly and without hysteresis.

The response of our device to cycles of RH between 30 and 90% was also studied. The results are shown in Fig. 5(b). Note also that in this case of our device provides again accurate information as an electronic humidity sensor.

To compensate the temperature effect on our sensor we need to understand the response of the polymer micro-cap to temperature. By differentiating Eq. (6) with respect to temperature we get [54]:

$$\frac{\partial \lambda_m}{\partial T} = \left[\frac{1}{n_p}\frac{\partial n_p}{\partial T} + \frac{1}{d}\frac{\partial d}{\partial T} \right] \lambda_m. \tag{8}$$

This means that temperature will cause a shift to λ_m. Thus, to compensate the temperature effect on our devices will be necessary to use two SMF with polymer microcaps, one of them must to be isolated from humidity.

The effect of temperature on the maximum of the interference pattern (λ_m) and on the RH sensitivity (S_{RH}) is calculated according to the two following equations:

$$\lambda_m(T) = 827,\ 6 + 0.254 \cdot T\,(\mathrm{nm/^oC}), \tag{9}$$

$$S_{RH}(T) = 0.148 - 0.0033 \cdot T + 5,\ 9E - 5 \cdot T^2\ (\mathrm{nm}\ /\%\mathrm{RH}). \tag{10}$$

Furthermore, the resolution of our sensor was found to be 0.04% RH.

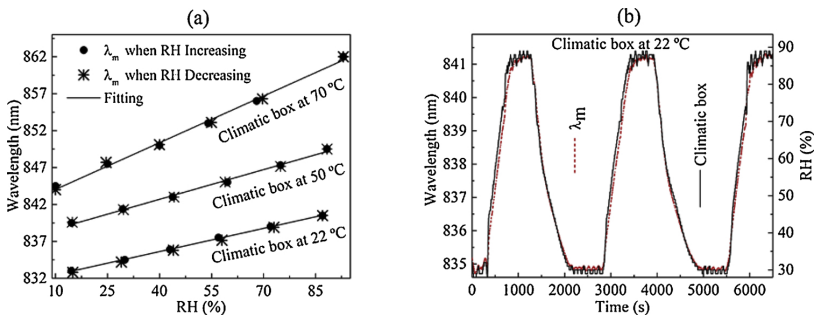

Fig. 5. (a) Plot of RH versus of λ_m at differents temperatures. At all temperatures the response of our sensor was linear and without hysteresis. (b) Response of our sensor when it is exposed to several cycles of RH variations from ~30 to ~90% at 22 °C.

5. Conclusions

We have reported on an accurate interferometric fiber optic humidity sensor which has miniature size. Experimentally, it has been shown to be as fast, accurate and sensitive as a commercial capacitive humidity sensor with which it has been compared. Our sensor provides linear response, broad humidity measuring range, and high sensitivity over the whole measuring range. The fabrication of the sensors is simple and reproducible. In our humidity sensor, the key element is an off-center polymer microcap bonded onto the polished facet of a single mode optical fiber. It can be possible compensate the temperature effect on the polymer by using two of our devices, one of them isolated from humidity.

We believe that the devices here proposed can be useful in miniature spaces where reliable and accurate humidity measurements are needed. Other applications that we foresee are in the field of bio-chemical sensing. In these applications, synthetized polymers with tailored optical and physical properties will be required. Then, under the presence of the parameters to sense, the interference pattern will change, and therefore will be detected or monitored with the techniques proposed in this work.

Acknowledgements

This work was funded by the Fondo Europeo de Desarrollo Regional (FEDER); the Ministerio de Economía y Competitividad (projects PGC2018-101997-B-I00 and RTI2018-094669-B-C31), and in part by the Gobierno Vasco/Eusko Jaurlaritza IT933-16 and ELKARTEK KK-2018/00078, (μ4Indust and SMARTRESNAK). Oskar Arrizabalaga acknowledges a PhD fellowship from the Departamento de Educación, Política Lingüística y Cultura del Gobierno Vasco/Eusko Jaurlaritza.

References

[1] W. Kastner, G. Neugschwandtner, S. Soucek, H.M. Newman, Communication systems for building automation and control, Proceedings of the IEEE 93 (6) (2005) 1178–1203, https://doi.org/10.1109/JPROC.2005.849726.

[2] T. Tatara, K. Tsuzaki, An apnea monitor using a rapid-response hygrometer, J. Clin. Monit. 13 (1) (1997) 5–9, https://doi.org/10.1023/A:1007380021895.

[3] B. Du, D. Yang, X. She, Y. Yuan, D. Mao, Y. Jiang, F. Lu, MoS_2-based all-fiber humidity sensor for monitoring human breath with fast response and recovery, Sens. Actuators B Chem. 251 (2017) 180–184, https://doi.org/10.1016/j.snb.2017.04.193.

[4] U. Mogera, A.A. Sagade, S.J. George, G.U. Kulkarni, Ultrafast response humidity sensor using supramolecular nanofibre and its application in monitoring breath humidity and flow, Sci. Rep. 4 (2014) 4103, , https://doi.org/10.1038/srep04103.

[5] C. Laville, C. Pellet, G. N'Kaoua, Interdigitated humidity sensors for a portable clinical microsystem, 1st Annual International IEEE-EMBS Special Topic Conference on Microtechnologies in Medicine and Biology - Proceedings (2000), https://doi.org/10.1109/MMB.2000.893849.

[6] W.P. Elliott, D.J. Gaffen, On the utility of radiosonde humidity archives for climate studies, Bull. Am. Meteorol. Soc. 72 (10) (1991) 1507–1520, https://doi.org/10.1175/1520-0477(1991)072<1507:OTUORH>2.0.CO;2.

[7] Y. Sakai, Y. Sadaoka, M. Matsuguchi, Humidity sensors based on polymer thin films, Sens. Actuators B Chem. 35 (1–3) (1996) 85–90, https://doi.org/10.1016/S0925-4005(96)02019-9.

[8] Z.-T. Zhu, J.T. Mason, R. Dieckmann, G.G. Malliaras, Humidity sensors based on pentacene thin-film transistors, Appl. Phys. Lett. 81 (24) (2002) 4643–4645, https://doi.org/10.1063/1.1527233.

[9] C.T. Wang, C.L. Wu, I.C. Chen, Y.H. Huang, Humidity sensors based on silica nanoparticle aerogel thin films, Sens. Actuators B Chem. 107 (1) (2005) 402–410, https://doi.org/10.1016/j.snb.2004.10.034.

[10] K.P. Yoo, L.T. Lim, N.K. Min, M.J. Lee, C.J. Lee, C.W. Park, Novel resistive-type humidity sensor based on multiwall carbon nanotube/polyimide composite films, Sensors and Actuators, B: Chemical. 145 (1) (2010) 120–125, https://doi.org/10.1016/j.snb.2009.11.041.

[11] W. Geng, X. He, Y. Su, J. Dang, J. Gu, W. Tian, Q. Zhang, Remarkable humidity-responsive sensor based on poly (N,N-diethylaminoethyl methacrylate)-b-poly-styrene block copolymers, Sens. Actuators B Chem. 226 (2016) 471–477, https://doi.org/10.1016/j.snb.2015.12.027.

[12] Y. Xiao, J. Zhang, X. Cai, S. Tan, J. Yu, H. Lu, Y. Luo, G. Liao, S. Li, J. Tang, Z. Chen, Reduced graphene oxide for fiber-optic humidity sensing, Opt. Express 22 (25) (2014) 31555–31567, https://doi.org/10.1364/OE.22.031555.

[13] X. Peng, J. Chu, B. Yang, P.X. Feng, Mn-doped zinc oxide nanopowders for humidity sensors, Sens. Actuators B Chem. 174 (2012) 258–262, https://doi.org/10.1016/j.snb.2012.07.011.

[14] I.R. Matias, F.J. Arregui, J.M. Corres, J. Bravo, Evanescent field fiber-optic sensors for humidity monitoring based on nanocoatings, IEEE Sens. J. 7 (1) (2007) 89–95, https://doi.org/10.1109/JSEN.2006.886889.

[15] Z. Zhao, Y. Duan, A low cost fiber-optic humidity sensor based on silica sol-gel film, Sensors and Actuators, B: Chemical. 160 (1) (2011) 1340–1345, https://doi.org/10.1016/j.snb.2011.09.072.

[16] S.W. James, R.P. Tatam, Optical fibre long-period grating sensors: characteristics and application, Meas. Sci. Technol. 14 (5) (2003) R49–R61, https://doi.org/10.1088/0957-0233/14/5/201.

[17] O. Ivanov, S. Nikitov, Y. Gulyaev, Cladding modes of optical fibers: properties and applications, Physics-Uspekhi. 49 (2) (2006) 117–224, https://doi.org/10.1070/PU2006v049n02ABEH005784.

[18] L. Alwis, T. Sun, V. Grattan Kenneth, Analysis of polyimide-coated optical relative humidity sensor, IEEE Sens. J. 7 (2) (2013) 767–771, https://doi.org/10.1109/JSEN.2012.2227714.

[19] L. Alwis, T. Sun, K.T.V. Grattan, Fibre optic long period grating-based humidity sensor probe using a Michelson interferometric arrangement, Sensors and Actuators, B: Chemical. 178 (1970) 694–699, https://doi.org/10.1016/j.snb.2012.11.062.

[20] M. Konstantaki, S. Pissadakis, S. Pispas, N. Madamopoulos, N.A. Vainos, Optical fiber long-period grating humidity sensor with poly(ethylene oxide)/cobalt chloride coating, Appl. Opt. 45 (19) (2006) 4567–4571, https://doi.org/10.1364/AO.45.004567.

[21] X. Yu, P. Childs, M. Zhang, Y. Liao, J. Ju, W. Jin, Relative humidity sensor based on cascaded long-period gratings with hydrogel coatings and Fourier demodulation, Ieee Photonics Technol. Lett. 21 (24) (2009) 1828–1830, https://doi.org/10.1109/LPT.2009.2034620.

[22] D. Viegas, J. Goicoechea, J.L. Santos, F.M. Araújo, L.A. Ferreira, F.J. Arregui, I.R. Matias, Sensitivity improvement of a humidity sensor based on silica nanospheres on a long-period fiber grating, Sensors. 9 (1) (2009) 519–527, https://doi.org/10.3390/s90100519.

[23] K.O. Hill, G. Meltz, Fiber Bragg grating technology fundamentals and overview, J. Light. Technol. 15 (8) (1997) 1263–1276, https://doi.org/10.1109/50.618320.

[24] N.A. David, P.M. Wild, N. Djilali, Parametric study of a polymer-coated fibre-optic humidity sensor, Meas. Sci. Technol. 46 (7) (2012) 032001–037001, https://doi.org/10.1088/0957-0233/23/3/035103.

[25] P. Kronenberg, P.K. Rastogi, P. Giaccari, H.G. Limberger, Relative humidity sensor with optical fiber Bragg gratings, Opt. Lett. 27 (16) (2002) 1385–1387, https://doi.org/10.1364/OL.27.001385.

[26] T.L. Yeo, T. Sun, K.T.V. Grattan, D. Parry, R. Lade, B.D. Powell, Characterisation of a polymer-coated fibre Bragg grating sensor for relative humidity sensing, Sens. Actuators B Chem. 110 (1) (2005) 148–156, https://doi.org/10.1016/j.snb.2005.01.033.

[27] Y. Lin, Y. Gong, Y. Wu, H. Wu, Polyimide-coated fiber Bragg grating for relative humidity sensing, Photonic Sens. 5 (1) (2015) 60–66, https://doi.org/10.1007/s13320-014-0218-8.

[28] A.J. Swanson, S.G. Raymond, S. Janssens, R.D. Breukers, M.D.H. Bhuiyan, J.W. Lovell-Smith, M.R. Waterland, Development of novel polymer coating for FBG based relative humidity sensing, Sens. Actuators A Phys. 249 (2016) 217–224, https://doi.org/10.1016/j.sna.2016.08.034.

[29] B.N. Shivananju, S. Yamdagni, R. Fazuldeen, A.K.S. Kumar, S.P. Nithin, M.M. Varma, S. Asokan, Highly sensitive carbon nanotubes coated etched fiber bragg grating sensor for humidity sensing, IEEE Sens. J. 14 (8) (2014) 2615–2619, https://doi.org/10.1109/JSEN.2014.2312353.

[30] G. Berruti, M. Consales, M. Giordano, L. Sansone, P. Petagna, S. Buontempo, G. Breglio, A. Cusano, Radiation hard humidity sensors for high energy physics applications using polyimide-coated fiber Bragg gratings sensors, Sens. Actuators B Chem. 177 (2013) 94–102, https://doi.org/10.1016/j.snb.2012.10.047.

[31] A.J. Swanson, S.G. Raymond, S. Janssens, R.D. Breukers, M.D.H. Bhuiyan, J.W. Lovell-Smith, M.R. Waterland, Investigation of polyimide coated fibre Bragg gratings for relative humidity sensing, Meas. Sci. Technol. 26 (12) (2015) 125001–127002, https://doi.org/10.1088/0957-0233/26/12/125101.

[32] L. Zhang, F. Gu, J. Lou, X. Yin, L. Tong, Fast detection of humidity with a sub-wavelength-diameter fiber taper coated with gelatin film, Opt. Express 16 (17) (2008) 13349–13353, https://doi.org/10.1364/OE.16.013349.

[33] J.M. Corres, F.J. Arregui, I.R. Matias, Design of humidity sensors based on tapered optical fibers, J. Light. Technol. 24 (11) (2006) 4329–4336, https://doi.org/10.1109/JLT.2006.883668.

[34] J.M. Corres, F.J. Arregui, I.R. Matías, Sensitivity optimization of tapered optical fiber humidity sensors by means of tuning the thickness of nanostructured sensitive coatings, Sens. Actuators B Chem. 122 (2) (2007) 442–449, https://doi.org/10.1016/j.snb.2006.06.008.

[35] J. Mathew, Y. Semenova, G. Rajan, G. Farrell, Humidity sensor based on photonic crystal fibre interferometer, Electron. Lett. 46 (19) (2010) 1341–1343, https://doi.org/10.1049/el.2010.2080.

[36] T. Li, X. Dong, C.C. Chan, K. Ni, S. Zhang, P.P. Shum, Humidity sensor with a PVA-coated photonic crystal fiber interferometer, IEEE Sens. J. 13 (6) (2013) 2214–2216, https://doi.org/10.1109/JSEN.2012.2234100.

[37] D. Lopez-Torres, C. Elosua, J. Villatoro, J. Zubia, M. Rothhardt, K. Schuster, F.J. Arregui, Photonic crystal fiber interferometer coated with a PAH/PAA nanolayer as humidity sensor, Sens. Actuators B Chem. 242 (2017) 1065–1072, https://doi.org/10.1016/J.SNB.2016.09.144.

[38] Y. Wang, C. Shen, W. Lou, F. Shentu, Fiber optic humidity sensor based on the graphene oxide/PVA composite film, Opt. Commun. 372 (2016) 229–234, https://doi.org/10.1016/j.optcom.2016.04.030.

[39] J. An, Y. Jin, M. Sun, X. Dong, Relative humidity sensor based on SMS fiber structure with two waist-enlarged tapers, IEEE Sens. J. 14 (8) (2014) 2683–2686, https://doi.org/10.1109/JSEN.2014.2313878.
[40] M. Consales, A. Buosciolo, A. Cutolo, G. Breglio, A. Irace, S. Buontempo, P. Petagna, M. Giordano, A. Cusano, Fiber optic humidity sensors for high-energy physics applications at CERN, Sens. Actuators B Chem. 159 (1) (2011) 66–74, https://doi.org/10.1016/j.snb.2011.06.042.
[41] M.Y. Mohd Noor, N.M. Kassim, A.S.M. Supaat, M.H. Ibrahim, A.I. Azmi, A.S. Abdullah, G.D. Peng, Temperature-insensitive photonic crystal fiber interferometer for relative humidity sensing without hygroscopic coating, Meas. Sci. Technol. 24 (10) (2013) 102001–107002, https://doi.org/10.1088/0957-0233/24/10/105205.
[42] M.R.K. Soltanian, A.S. Sharbirin, M.M. Ariannejad, I.S. Amiri, R.M. De La Rue, G. Brambilla, B.M.A. Rahman, K.T.V. Grattan, H. Ahmad, Variable waist-diameter mach-zehnder tapered-fiber interferometer as humidity and temperature sensor, IEEE Sens. J. 16 (15) (2016) 5987–5992, https://doi.org/10.1109/JSEN.2016.2573961.
[43] C. Huang, W. Xie, D. Lee, C. Qi, M. Yang, M. Wang, J. Tang, Optical Fiber humidity sensor with porous TiO2/SiO2/TiO2 coatings on Fiber tip, Ieee Photonics Technol. Lett. 27 (14) (2015) 1495–1498, https://doi.org/10.1109/LPT.2015.2426726.
[44] F. Mitschke, Fiber-optic sensor for humidity, Opt. Lett. 14 (17) (1989) 967–969, https://doi.org/10.1364/OL.14.000967.
[45] F.J. Arregui, Y. Liu, I.R. Matias, R.O. Claus, Optical fiber humidity sensor using a nano Fabry-Perot cavity formed by the ionic self-assembly method, Sensors and Actuators, B: Chemical. 59 (1) (1999) 54–59, https://doi.org/10.1016/S0925-4005(99)00232-4.
[46] M. Yang, J. Peng, T. Sun, W. Wang, Y. Qu, Thin-film-based optical fiber Fabry–Perot interferometer used for humidity sensing, Appl. Opt. 57 (12) (2018) 2967–2972, https://doi.org/10.1364/ao.57.002967.
[47] J. Shi, D. Xu, W. Xu, Y. Wang, C. Yan, C. Zhang, D. Yan, Y. He, L. Tang, W. Zhang, T. Liu, J. Yao, Humidity Sensor Based on Fabry-Perot Interferometer and Intracavity Sensing of Fiber Laser, J. Light. Technol. 35 (21) (2017) 4789–4795, https://doi.org/10.1109/JLT.2017.2750172.
[48] J.S. Santos, I.M. Raimundo, C.M.B. Cordeiro, C.R. Biazoli, C.A.J. Gouveia, P.A.S. Jorge, Characterisation of a Nafion film by optical fibre Fabry-Perot interferometry for humidity sensing, Sens. Actuators B Chem. 196 (2014) 99–105, https://doi.org/10.1016/j.snb.2014.01.101.
[49] C.-L. Lee, Y.-W. You, J.-H. Dai, J.-M. Hsu, J.-S. Horng, Hygroscopic polymer microcavity fiber Fizeau interferometer incorporating a fiber Bragg grating for simultaneously sensing humidity and temperature, Sens. Actuators B Chem. 222 (2016) 339–346, https://doi.org/10.1016/j.snb.2015.08.086.
[50] S. Wu, G. Yan, Z. Lian, X. Chen, B. Zhou, S. He, An open-cavity Fabry-Perot interferometer with PVA coating for simultaneous measurement of relative humidity and temperature, Sens. Actuators B Chem. 225 (2016) 50–56, https://doi.org/10.1016/j.snb.2015.11.015.
[51] L.H. Chen, T. Li, C.C. Chan, R. Menon, P. Balamurali, M. Shaillender, B. Neu, X.M. Ang, P. Zu, W.C. Wong, K.C. Leong, Chitosan based fiber-optic Fabry–Perot humidity sensor, Sens. Actuators B Chem. 169 (2012) 167–172, https://doi.org/10.1016/j.snb.2012.04.052.
[52] A. Lopez Aldaba, D. Lopez-Torres, C. Elosua, J.L. Auguste, R. Jamier, P. Roy, F.J. Arregui, M. Lopez-Amo, SnO_2-MOF-Fabry-Perot optical sensor for relative humidity measurements, Sens. Actuators B Chem. 257 (2018) 189–199, https://doi.org/10.1016/j.snb.2017.10.149.
[53] B. Wang, J. Tian, L. Hu, Y. Yao, High sensitivity humidity fiber-optic sensor based on all-agar fabry–Perot interferometer, IEEE Sens. J. 18 (12) (2018) 4879–4885, https://doi.org/10.1109/JSEN.2018.2828134.
[54] O. Arrizabalaga, G. Durana, J. Zubia, J. Villatoro, Accurate microthermometer based on off center polymer caps onto optical fiber tips, Sens. Actuators B Chem. 272 (2018) 612–617, https://doi.org/10.1016/j.snb.2018.05.148.
[55] Y. St-Amant, D. Gariépy, D. Rancourt, Intrinsic properties of the optical coupling between axisymmetric Gaussian beams, Appl. Opt. 43 (30) (2004) 5691–5704, https://doi.org/10.1364/AO.43.005691.
[56] P.R. Wilkinson, J.R. Pratt, Analytical model for low finesse, external cavity, fiber Fabry–Perot interferometers including multiple reflections and angular misalignment, Appl. Opt. 50 (23) (2011) 4671–4680, https://doi.org/10.1364/AO.50.004671.
[57] D. Su, X. Qiao, Q. Rong, H. Sun, J. Zhang, Z. Bai, Y. Du, D. Feng, Y. Wang, M. Hu, Z. Feng, A fiber Fabry–Perot interferometer based on a PVA coating for humidity measurement, Opt. Commun. 311 (2013) 107–110, https://doi.org/10.1016/J.OPTCOM.2013.08.016.
[58] S. Nemoto, T. Makimoto, Analysis of splice loss in single-mode fibres using a Gaussian field approximation, Opt. Quantum Electron. 11 (5) (1979) 447–457, https://doi.org/10.1007/BF00619826.
[59] G. Baschek, G. Hartwig, F. Zahradnik, Effect of water absorption in polymers at low and high temperatures, Polymer. 40 (12) (1999) 3433–3441, https://doi.org/10.1016/S0032-3861(98)00560-6.